Climate Dynamics

DOI 10.1007/s00382-002-0270-8

Constraining temperature variations over the last millennium by comparing simulated and observed atmospheric CO_2

S. Gerber · F. Joos(✉) · P. Brügger · T. F. Stocker · M. E. Mann · S. Sitch · M. Scholze

S. Gerber · F. Joos · P. Brügger · T.F. Stocker
Physics Institute, Climate and Environmental Physics, Sidlerstrasse 5 University of Bern, Bein-CH-31012 Switzerland

M.E. Mann
Department of Environmental Sciences, University of Virginia, USA

S. Sitch
Potsdam Institute for Climate Impact Research, Potsdam, Germany

M. Scholze
Max Planck Institute for Meteorology, Hamburg, Germany

✉ E-mail: joos@climate.unibe.ch

Received: 6 March 2002 / **Accepted:** 17 June 2002

Abstract. The response of atmospheric CO_2 and climate to the reconstructed variability in solar irradiance and radiative forcing by volcanoes over the last millennium is examined by applying a coupled physical-biogeochemical climate model that includes the Lund-Potsdam-Jena dynamic global vegetation model (LPJ-DGVM) and a simplified analogue of a coupled atmosphere-ocean general circulation model. The modeled variations of atmospheric CO_2 and Northern Hemisphere (NH) mean surface temperature are compatible with reconstructions from different Antarctic ice cores and temperature proxy data. Simulations where the magnitude of solar irradiance changes is increased yield a mismatch between model results and CO_2 data, providing evidence for modest changes in solar irradiance and global mean temperatures over the past millennium and arguing against a significant amplification of the response of global or hemispheric annual mean temperature to solar forcing. Linear regression (r = 0.97) between modeled changes in atmospheric CO_2 and NH mean surface temperature yields a CO_2 increase of about 12 ppm for a temperature increase of 1 °C and associated precipitation and cloud cover changes. Then, the CO_2 data range of 12 ppm implies that multi-decadal NH temperature changes between 1100 and 1700 AD had to be within 1 °C. Modeled preindustrial variations in atmospheric $\delta^{13}C$ are small compared to the uncertainties in ice core $\delta^{13}C$ data. Simulations with natural forcings only suggest that atmospheric CO_2 would have remained

around the preindustrial concentration of 280 ppm without anthropogenic emissions. Sensitivity experiments show that atmospheric CO_2 closely follows decadal-mean temperature changes when changes in ocean circulation and ocean-sediment interactions are not important. The response in terrestrial carbon storage to factorial changes in temperature, the seasonality of temperature, precipitation, and atmospheric CO_2 has been determined.

1

Introduction

Ice core data of the atmospheric CO_2 history provide information on the coupled climate-carbon cycle system. Estimates of past temperature and climate variability are a prerequisite for a possible attribution of the twentieth century warming to anthropogenic greenhouse gas forcing. While proxy based climate reconstructions can inform our knowledge of large-scale temperature variations in past centuries, they are not without their uncertainties (Folland et al. *2001*). Independent estimates from models driven with estimates of changes in radiative forcing can provide a complementary picture of temperature trends over the past millennium (e.g., Crowley *2000*). Here, we make use of atmospheric CO_2 variations as recorded in ice cores in the context of a modeling approach that is as yet a new constraint on temperature variations over the last millennium.

Magnitude and importance of fundamental mechanisms operating in the climate carbon cycle system such as the role of solar variability in climate change or the dependency of primary productivity on atmospheric CO_2 are under debate. A reason is that time scales larger than a few years cannot be assessed by detailed and well controlled field studies and that long-term instrumental observations are missing for many variables. On the other hand, paleoclimatic reconstructions provide the opportunity to test our understanding and models of the Earth system on long time scales. However, paleoclimatic studies generally suffer from incomplete data and uncertainties in reconstructed data. In this study, we will use the radiative forcing, temperature, and CO_2 data shown in Fig. 1 to investigate whether our current understanding of variations in climate (Folland et al. *2001*) and the global carbon cycle (Prentice et al. *2001*) is consistent with the ice core CO_2 record (Stauffer et al. *2002*) by forcing the reduced-form Bern carbon cycle-climate (Bern CC) model (Joos et al. *2001*) with reconstructed changes in radiative forcing from variations in solar irradiance and volcanic eruptions (Bard et al. *2000*; Crowley *2000*).

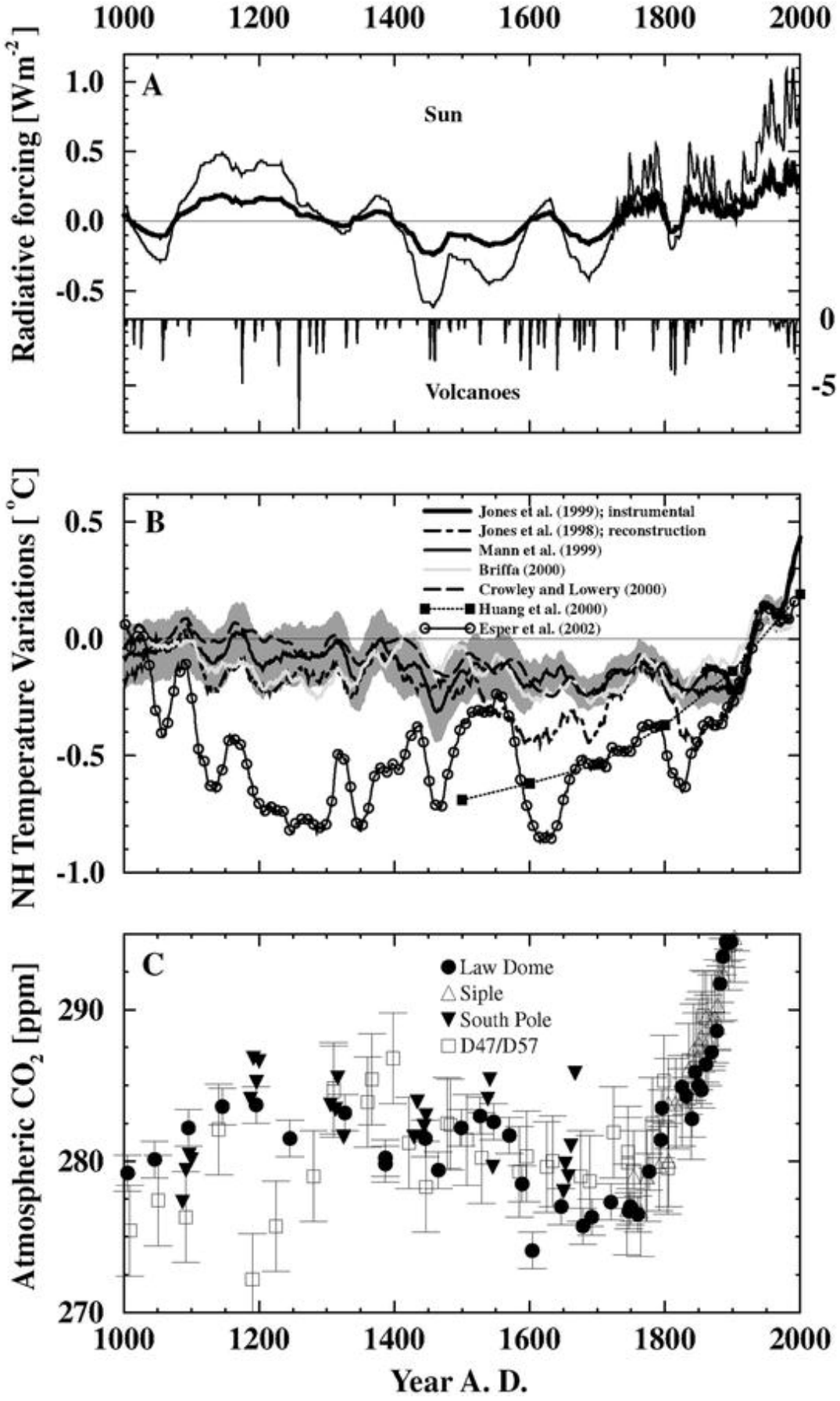
1000
1200
1400
1600
1800
2000
A
Sun
Volcanoes
Radiative forcing [Wm-2]
1.0
0.5
0.0
-0.5
0
-5
B
Jones et al. (1999); instrumental
Jones et al. (1998); reconstruction
Mann et al. (1999)
Briffa (2000)
Crowley and Lowery (2000)
Huang et al. (2000)
Esper et al. (2002)
NH Temperature Variations [°C]
0.5
0.0
-0.5
-1.0
C
Law Dome
Siple
South Pole
D47/D57
Atmospheric CO2 [ppm]
290
280
270
Year A. D.

Fig. 1A-C. Reconstructions of solar and volcanic radiative forcing, NH temperature, and atmospheric CO_2 for the last millennium. **A** *top panel*: reconstructed radiative forcing from variations in total solar irradiance based on a smoothed cosmonuclides production record (Bard et al. *2000*). The different curves have been obtained with different scaling factors to match the Maunder Minimum (around 1700) irradiance reduction derived by Reid (*1997*) (*thin solid line*) and by Lean et al. (*1995*) (*thick solid line*). This latter reconstruction has been used as standard input in this study. High-frequency variations have been included here for the industrial period based on Lean et al. (*1995*). **A** *Bottom panel, right hand axis*: reconstructed radiative forcing from explosive volcanic eruptions (Crowley *2000*). Note the *different scales* between the upper and lower panel. **B** Reconstructions of Northern Hemisphere (NH) surface temperature variations for the last millennium by Jones et al. (*1998*) (*dot-dashed*, summer, extratropical-emphasis), Mann et al. (*1999*) (*thin solid line* annual mean, full hemisphere), Briffa (*2000*) (*gray*, summer, extra-tropical) Crowley and Lowery (*2000*)(*dashed*, summer-emphasis, extratropical), Huang et al. (*2000*) (*squares*, borehole temperature, gridded before averaging, taken from Briffa and Osborn (*2002*)) and Esper et al. (*2002*) (*solid line*, with *circles*). The instrumental record (annual mean, full hemisphere) is shown by the *thick solid line* (Jones et al. *1999*). All series have been smoothed by 31-year running averages. The *shaded area* indicates the uncertainty (±2 standard deviation) of the smoothed temperature reconstruction by Mann et al. (*1999*). It was computed based on the use of the standard reduction of variance in the estimate of the mean, $\bar{\sigma} = \sqrt{\sigma^2/N'}$ where σ^2 is the nominal variance in the annual estimates diagnosed from the calibration residuals, and N' is the effective degrees of freedom which is approximately $N' = N/2$ in the decadal range, owing to the existence of serial correlation in the calibration residuals. **C** Atmospheric CO_2 concentration as measured on air entrapped in ice drilled at Law Dome (*solid circles*) (Etheridge et al. *1996*), Siple (*open triangles*) (Neftel et al. *1985*), South Pole (*solid triangles*) (Siegenthaler et al. *1988*), and Adelie Land (cores D47 and D57, *open squares*) (Barnola et al. *1995*). The age scale of the South Pole ice core has been shifted by 115 years towards older dates compared to the original publication based on an improved firn-diffusion model (Schwander *1996*)

In the following paragraphs, we will discuss the data shown in Fig. 1 that serve as the primary input to our study. Proxy data from different archives such as trees, lakes and ocean sediments, corals, boreholes, ice cores and historical documentary evidence reveal variations in climate during the last millennium (Esper et al. *2002*; Folland et al. *2001*; Hu et al. *2001*; Johnsen et al. *2001*; Kreutz et al. *1997*; Mann et al. *1998*, *1999*; Pfister et al. *1996*; Pfister *1999*) that are linked to variations in solar irradiance (e.g., Crowley *2000*; Bond et al. *2001*) and to explosive volcanic eruptions (e.g., Briffa et al. *1998*), as well as to variations in greenhouse gas concentrations.

Reconstructions of solar irradiance (Fig. 1A, upper panel) show a high total solar irradiance (TSI) during the 11th and 12th century, and low TSI during 1400 to 1700 AD. Distinct minima are found around 1320, 1450, 1550, 1680 and 1820 AD. Volcanic forcing (Fig. 1A, lower panel) is negative (cooling) and pulse-like as sulfur injected into the stratosphere by explosive eruptions is removed within a few years. Uncertainties in reconstructed radiative forcing, that serves as an input to drive climate models, are large. For example, the role of solar variability for climate change has been discussed controversially (Ramaswamy et al. *2001*). Changes in TSI are reconstructed based on proxy records of solar magnetic activity such as historically observed sunspot numbers and the abundance of the cosmogenic radio-isotopes ^{10}Be as recorded in polar ice and ^{14}C as recorded in tree rings (e.g., Beer et al. *1994*; Bard et al. *2000*). Simple linear scaling has been applied to translate the radio-isotope records into TSI changes by Bard et al. (*2000*) and the scaling varies by a factor of 2.6 between different plausible reconstructions (Fig. 1A). In addition to TSI variations, changes in ultraviolet radiation influence the atmospheric ozone distribution and thereby climate (Haigh *1996*; Thompson

and Solomon *2002*). Furthermore, it has been speculated that changes in solar magnetic activity itself influence climate (Svensmark and Friis-Christensen *1997*). Similar uncertainties exist with regard to past volcanic forcing.

Reconstructions of the Northern Hemisphere (NH) mean surface temperature show distinct cold and warm periods during the past millennium (Fig. 1B). Most reconstructions suggest that NH mean temperature was lower than today by a few tenths of a degree (Folland et al. *2001*). A recent primarily extratropical reconstruction (Esper et al. *2002*) yields more pronounced temperature fluctuations and suggests that NH temperatures have been lower by 0.3 to 1 °C between 1200 AD and 1800 AD as compared to recent decades and a warm period around 1000 AD. The timing of cold and warm periods varies considerably over the globe (Folland et al. *2001*). Unusually cold and dry winters have been found in Central Europe during the "Little Ice Age" that were associated with lower index states of the Arctic and North Atlantic Oscillation patterns during the seventeenth century (Wanner et al. *1995*; Luterbacher et al. *1999*). On the other hand, recent work by Hendy et al. (*2002*) suggest little if any cooling at all during the seventeenth to nineteenth centuries in the Great Barrier Reef sector of the tropical Pacific. Primarily extratropical NH temperature reconstructions exhibit more cooling during the seventeenth to nineteenth centuries than reconstructions based on the full (tropical and extratropical) NH (see e.g., Mann et al. *1999*; Crowley and Lowery *2000*; Folland et al. *2001*; Esper et al. *2002*). Measurements of borehole temperatures (Huang et al. *2000*) reveal a warming of 0.9 °C since 1500 AD. Simulations with energy balance models (Crowley *2000*; Bertrand et al. *2002*) and atmosphere-ocean general circulation models (Cubasch et al. *1997*; Shindell et al. *2001*) forced by reconstructed radiative forcing yield small changes in hemispheric mean surface temperature and are in broad agreement with the reconstructed small changes by Mann et al. (*1999*) or Briffa (*2000*), but in conflict with results from Esper et al. (*2002*). There remain substantial uncertainties (e.g., Folland et al. *2001*) in existing reconstructions and differences between published reconstructions of NH mean surface temperature are up to 0.8 °C (Fig. 1B). In conclusion, uncertainties in past climate forcing and climate reconstructions call for independent additional information to further constrain past global climate variations.

Variations in atmospheric tracers recorded in ice cores such as carbon dioxide, methane, nitrous oxide, and sulfate provide additional clues on the magnitude of past climate changes. The ice core records show a small variability in atmospheric greenhouse gases and deposited sulfate over the last millennium until the onset of industrialization as compared to measured variations over glacial-interglacial cycles, Dansgaard/Oeschger events, or the entire Holocene (Stauffer et al. *2002*; Bigler et al. *2002*). Qualitatively, this suggests that averaged over the globe or the NH natural climate variations have been modest during the last millennium.

CO_2 data from several Antarctic ice cores (Fig. 1C) show that atmospheric CO_2 varied by less than 15 ppm during the last millennium until the onset of industrialization (Siegenthaler et al. *1988*; Barnola et al. *1995*; Etheridge et al. *1996*). However, the detailed evolution is not consistent between different cores. For example, results from cores D47/D57 (Barnola et al. *1995*) suggest an increase in atmospheric CO_2 of around 10 ppm during 1200 to 1400 AD, whereas the data from Law Dome (Etheridge et al. *1996*) suggest a small downward trend. Similarly, the Law Dome data show a rapid CO_2 decrease of about 8 ppm at the end of the sixteenth century, which is not found in the other cores. Possible reasons for these discrepancies are the in-situ transformation of calcite and/or organic carbon to CO_2 after the enclosure of air in the ice (Tschumi and Stauffer *2000*; Anklin et al. *1995*) as well as analytical problems, especially for measurements made in the 1980 and early 1990s. In summary, preindustrial atmospheric CO_2 variations were small during the last millennium and details in the different CO_2 ice core records need to be interpreted with caution.

The outline of this work is as follows. The Bern CC model and the experimental setup are described in the next section. In Sect. 3.1 we present the sensitivity of the terrestrial component of the Bern CC model, the Lund-Potsdam-Jena Dynamic Global Vegetation Model (LPJ-DGVM), to step-like changes in one of the driving variables CO_2, temperature, precipitation and cloud cover. The adjustment time of atmospheric CO_2 to a step change in radiative forcing or in climate is explored in Sect. 3.2 for the coupled carbon cycle-climate model. The results of the transient simulations for the past millennium are presented in Sects. 3.3 and 3.4. In Sect. 3.5, we apply the ice core CO_2 record to constrain low-frequency variations in NH mean surface temperature for the period 1100 to 1700 AD. In Sect. 3.6, we then compare simulated atmospheric $\delta^{13}C$ with ice core data and discuss briefly the relevance of $\delta^{13}C$ in the climate-carbon cycle system. Discussion and conclusions follow in Sect. 4.

2

Model description

The Bern CC model (Joos et al. *2001*) consists of a chemistry, radiative forcing, climate, and carbon cycle module. The main features of the model are summarized.

2.1

Radiative forcing

In simulations over the last millennium (1075 AD to 2000 AD), global-average radiative forcing from solar irradiance changes and explosive volcanic eruptions are prescribed (Crowley *2000*, Fig. 1A) to simulate the evolution of temperature, precipitation, cloud cover, and atmospheric CO_2. Radiative forcing by CO_2 is calculated from concentrations assuming a logarithmic relationship (Myhre et al. *1998*). Radiative forcing by other anthropogenic greenhouse gases and aerosols and carbon emissions due to fossil fuel use and land use changes for the industrial period (1700 to 2000 AD) are taken into account (Joos et al. *2001*).

2.2

Climate model

The model's climate component is an impulse response-empirical orthogonal function (IRF-EOF) substitute driven by radiative forcing. An IRF for surface-to-deep tracer mixing in combination with an equation describing air-sea heat exchange and the energy balance at the surface (Joos and Bruno *1996*) characterize the adjustment time of the climate system to changes in radiative forcing, whereas EOFs describe the spatial patterns of the annual mean perturbations in temperature (ΔT), precipitation (ΔP), and cloud cover (ΔCC) (Hooss et al. *2001*; Meyer et al. *1999*). The climate sensitivity for temperature, defined as the change in global mean surface temperature per radiative forcing unit, is specified here as a term in the surface energy balance equation (Siegenthaler and Oeschger *1984*), whereas the climate sensitivity of comprehensive models is determined by the strength of the resolved feedback mechanisms. The spatial patterns (EOFs) in ΔT, ΔP, and ΔCC associated with global temperature changes resulting from radiative forcing by greenhouse gases and solar irradiance were derived from a 850-year "$4 \times CO_2$" simulation with the ECHAM3/LSG model

wherein atmospheric CO_2 was quadrupled in the first 120 years and held constant thereafter (Voss and Mikolajewicz *2001*). The IRF for surface-to-deep mixing of heat (and other tracers) was derived from

the High-Latitude Exchange-Interior Diffusion/Advection (HILDA) model (Joos et al. *1996*). The combination of an IRF for surface-to-deep heat mixing and an energy balance equation allows us to explicitly simulate the damping effect of ocean heat uptake on modeled surface temperatures (Hansen et al. *1984*), in contrast to the IRF-EOF model developed by Hooss et al. (*2001*) that was used in earlier work with the Bern CC model (Joos et al. *2001*). Simulations with both IRF approaches yield almost identical results for the 4 $\times$ CO_2 experiment when the IRF-EOF models' climate sensitivity

for a doubling of atmospheric CO_2 is set to 2.5 °C, i.e., the sensitivity of the ECHAM3/LSG. However, when the IRF models' climate sensitivity is increased, temperature changes scale with the climate sensitivity in the IRF approach by Hooss et al. (*2001*), whereas in the IRF model used here simulated temperature changes are smaller during the first transient phase of the experiment, because ocean heat uptake is explicitly simulated.

Modeled changes in precipitation and cloud cover are used in a purely diagnostic way and scale linearly with the modeled global mean surface temperature changes. The climate sensitivities of the substitute for a doubling of atmospheric CO_2 corresponding to a change in radiative forcing of 3.7 W m^{-2} are 2.5 °C (global mean surface-air temperature), 64 mm yr^{-1} (global mean precipitation), and -0.9% (cloud cover) in the standard case. In sensitivity experiments, temperature sensitivities of 1.5 °C and 4.5 °C have been used; the sensitivities of other climate variables were scaled accordingly. We note that for the ECHAM3/LSG pattern deviations in NH mean are 20% larger than in global mean surface temperature and that the temperature deviations averaged over land are 36% higher than those averaged over the globe.

The temperature response of each volcanic eruption of the last millennium was calculated by multiplying its peak radiative forcing (Crowley *2000*) with an observationally based response pattern for tropical and high-latitude volcanoes, respectively. The temperature anomalies due to volcanic forcing were then linearly combined with the anomalies calculated by the ECHAM-3/LSG substitute in response to solar and CO_2 forcing. Changes in precipitation and photosynthetic active radiation in response to explosive volcanic eruptions were neglected. Each peak of the volcanic radiative forcing series was assigned to either a high latitude or a tropical eruption using a catalogue of volcanic eruptions (Simkin and Siebert *1994*). The average temperature response of tropical and northern high-latitude volcanoes was calculated from observations (Jones *1994*) following Robock and Mao (*1993*). First, low-frequency variations, and the El Niño/Southern Oscillation signal are removed from the temperature data and the resulting temperature anomalies are seasonally averaged. Then, the seasonal temperature anomalies for the first five years after the eruptions of the tropical volcanoes Krakatau (1883), Soufrière (1902)/Santa Maria (1902), El Chichón (1982), and Mt. Pinatubo (1991) were extracted. The individual seasonal temperature fields of the four eruptions were averaged for each year after the eruptions to obtain a five-year long data set. Finally, the anomalies were divided by the average of the peak radiative forcing of the four eruptions. The response of northern high-latitude volcanoes was obtained by repeating this procedure for the eruptions of Bandai (1888), Katmai (1912) and Bezymianny (1956). Peak radiative forcing of Bandai, which left no trace in the Crowley (*2000*) series, was calculated using the global-average aerosol optical depth estimate of Sato and Hansen (*1992*) and the relation of Lacis et al. (*1992*). We note that conclusions remain unchanged if the climatic response (temperature, precipitation, cloud cover) to explosive volcanic eruptions is calculated using the ECHAM3/LSG substitute instead of applying the observationally based temperature response pattern.

2.3

Carbon cycle model

The carbon cycle component consists of a well-mixed atmosphere, a substitute of the HILDA ocean model (Siegenthaler and Joos *1992*; Joos et al. *1996*), and the LPJ-DGVM (Sitch *2000*; Prentice et al. *2000*; Cramer et al. *2001*; Joos et al. *2001*; McGuire et al. *2001*; Sitch et al. submitted 2002; Kaplan *2002*). Surface-to-deep tracer transport in the ocean substitute is described by an IRF. The non-linearities in air-sea gas exchange and carbon chemistry are captured by separate equations. The effect of sea-surface warming on carbonate chemistry is included (Joos et al. *1999b*). However, ocean circulation changes are not considered in our standard simulation.

The LPJ-DGVM is driven by local temperatures, precipitation, incoming solar radiation, cloud cover, and atmospheric CO_2. The LPJ-DGVM simulates the distribution of nine plant functional types (PFTs) based on bioclimatic limits for plant growth and regeneration and plant-specific parameters that govern plant competition for light and water. The PFTs considered are tropical broad-leaved evergreen trees, tropical broad-leaved raingreen trees, temperate needle-leaved evergreen trees, temperate broad-leaved evergreen trees, temperate broad-leaved summergreen trees, boreal needle-leaved evergreen trees, boreal summergreen trees, C_3 grasses/forbs, and C_4 grasses. Dispersal processes are not explicitly modeled and an individual PFT can invade new regions if its bioclimatic limits and competition with other PFTs allow establishment. There are seven carbon pools per PFT, representing leaves, sapwood, heartwood, fine-roots, a fast and a slow decomposing above-ground litter pool, and a below-ground litter pool; and two soil carbon pools, which receive input from litter of all PFTs. Photosynthesis is as a function of absorbed photosynthetically active radiation, temperature, atmospheric CO_2 concentration, day length, and canopy conductance using a form of the Farquhar scheme (Farquhar et al. *1980*; Collatz et al. *1992*) with leaf-level optimized nitrogen allocation (Haxeltine and Prentice *1996*) and an empirical convective boundary layer parametrization (Monteith *1995*) to couple the carbon and water cycles. Soil texture classes are assigned to every grid cell (Zobler *1986*), and the soil hydrology is simulated using two soil layers (Haxeltine and Prentice *1996*). Decomposition rates of soil and litter organic carbon depend on soil temperature (Lloyd and Taylor *1994*) and moisture (Foley *1995*). Fire fluxes are calculated based on litter moisture content, a fuel load threshold, and PFT specific fire resistances (Thonicke et al. *2001*). ^{13}C discrimination during photosynthesis is based on Lloyd and Farquhar (*1994*). The spatial resolution of the LPJ-DGVM is set to 3.75° × 2.5°.

2.4

Model spin-up

The LPJ-DGVM is spun up from bare ground under pre-industrial CO_2 (281.43 ppm) and a baseline climate that includes inter-annual variability (Cramer et al. *2001*; Leemans and Cramer *1991*) for 2000 years for idealized sensitivity runs with the LPJ-DGVM alone and for 4000 years for simulations with the coupled climate-carbon cycle model. At year 400, the sizes of the slowly overturning soil carbon pools are calculated analytically from annual litter inputs and annual mean decomposition rates in order to reduce the necessary time to approach the final equilibrium. Then spin-up is continued and all pools (including the soil pools) and state variables are continuously updated. The annual average global net ecosystem production is less than $1 \cdot 10^{-2}$ gigatons of carbon (GtC) after 2000 years and less than $5 \cdot 10^{-3}$ GtC after 4000 years of spin-up. In standard simulations the LPJ-DGVM is coupled to the other modules after spin-up, and the spatial fields in annual mean perturbations of temperature, cloud cover, and precipitation simulated by the ECHAM3/LSG substitute and calculated for explosive volcanic eruptions are added to the baseline climate.

3

Results

3.1

Sensitivity of the dynamic global vegetation model to changes in temperature, precipitation, and atmospheric CO_2

In this section, the sensitivity of the LPJ-DGVM to spatially uniform step-like variations in temperature, precipitation, and atmospheric CO_2, is investigated to determine the importance of individual climate forcing factors for modeled terrestrial carbon storage. In the idealized sensitivity experiments presented here, the LPJ-DGVM is run alone and atmospheric CO_2 and climate are prescribed. A globally or hemispherically uniform perturbation in one of the driving variables (CO_2, temperature, precipitation) is added to the baseline climatology and simulations are continued until a new equilibrium is reached. Results are expressed as deviations to a baseline simulation. Experimental setup and results are summarized in Table 1.

Table 1. Equilibrium sensitivity of the terrestrial carbon storage to atmospheric CO_2 concentrations and climate parameters

Experiment	ΔCO_2	ΔT	ΔS_T	ΔP	ΔC_{terr}	γ
	[ppm]	[°C]	[%]	[%]	[GtC]	
Changes in atmospheric CO_2						
$S_{C\text{-}5}$	-5				-20	4.0 GtC/ppm
S_{C+5}	+5				+23	4.6 GtC/ppm
S_{C+10}	+10				+47	4.7 GtC/ppm
S_{C+250}	+250				+770	3.1 GtC/ppm
S_{C+500}	+500				+1220	2.4 GtC/ppm
S_{C+1000}	+1000				+1740	1.7 GtC/ppm
S_{C+2000}	+2000				+2280	1.1 GtC/ppm
Changes in temperature						
$S_{T\text{-}1}$		-1			+75	-75.0 GtC/°C
S_{T+1}		+1			-65	-65.0 GtC/°C
$S_{T\pm}1$		±1			+27	±27.0 GtC/°C
Changes in the seasonality of temperature						
S_{S+10}			+10		+22	2.2 GtC/%
$S_{S\text{-}10}$			-10		+66	6.6 GtC/%
Changes in precipitation						
$S_{P\text{-}20}$				-20	-130	6.5 GtC/%
$S_{P\text{-}14}$				-14	-90	6.4 GtC/%
$S_{P\text{-}8}$				-8	-51	6.4 GtC/%
$S_{P\text{-}2}$				-2	-12	6.0 GtC/%
S_{P+2}				+2	+12	6.0 GtC/%
S_{P+8}				+8	+42	5.3 GtC/%
S_{P+14}				+14	+68	4.9 GtC/%
S_{P+20}				+20	+100	5.0 GtC/%

In all sensitivity experiments, one driving variable was changed in a step-like manner while keeping all other variables constant and the model was run until the new equilibrium was reached. The last two columns give the total perturbation in terrestrial carbon storage (ΔC_{terr}) and the sensitivity (γ)

expressed as change in carbon storage per unit change in a driving variable. In experiments $S_{C\text{-}5}$ to S_{C+2000} atmospheric CO_2 was varied by -5 ppm to +2000 ppm. In experiments S_T and S_P

temperature and precipitation was varied uniformly over the globe, except in $S_{T\pm1}$, where temperature are decreased in the NH and increased in the Southern Hemisphere by 1 °C. Temperature seasonality was varied in experiments S_S

3.1.1

Temperature

The sensitivity of the LPJ-DGVM to variations in temperature is examined with step-like global temperature perturbations by +1 °C and -1 °C, respectively (experiments S_{T+1} and $S_{T\text{-}1}$). A third experiment $S_{T\pm1}$ is a sudden temperature decrease by 1 °C for all grid cells in the NH, and a simultaneous increase by 1 °C in the Southern Hemisphere (SH) to schematically mimic the effect of a reduction in the North Atlantic thermohaline circulation. We note, however, that paleodata and models suggest that for a reduction in the North Atlantic thermohaline circulation SH warming is much less pronounced than cooling in the Atlantic region. The atmospheric CO_2 is set to a constant value of 281 ppm. An increase in temperature leads to higher turnover rates of litter and soils and thus to a decrease in soil and litter carbon storage, whereas the effects on vegetation growth and vegetation structure vary regionally. With the experiment S_{T+1}, the terrestrial biosphere releases 65 GtC into the atmosphere until the new equilibrium is reached (Fig. 2). The overshooting immediately after the temperature perturbation (the stock is reduced by 83 GtC in the year 150) and the following approach towards the equilibrium state is governed by significant changes in vegetation distribution, especially in northern mid- and high-latitudes, and the long response time of slow overturning soils. The increase in carbon stock resulting from experiment $S_{T\text{-}1}$ is 75 GtC.

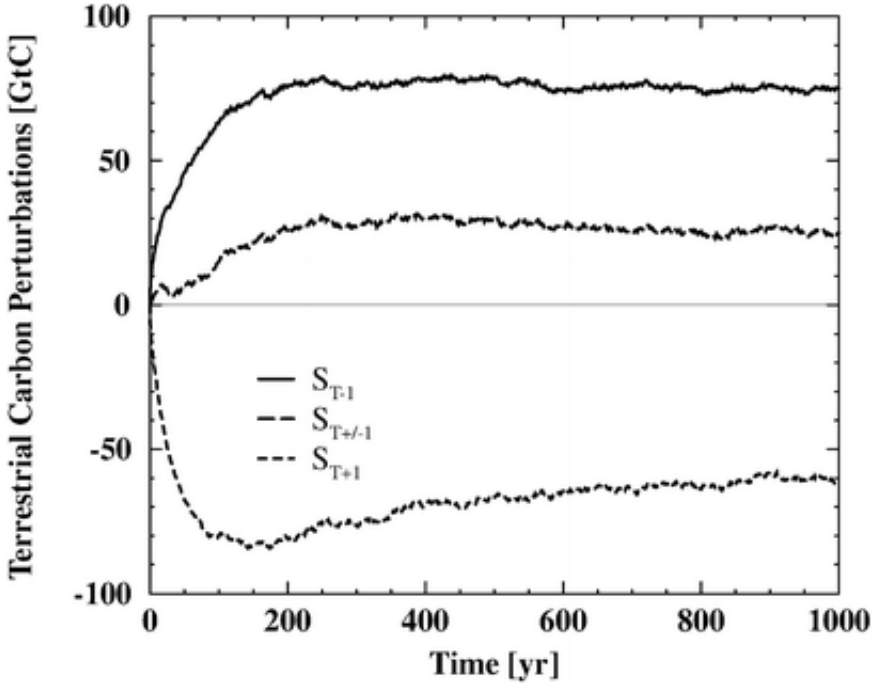

Fig. 2. Perturbations in terrestrial carbon inventories after a step change in air temperature. The *solid line* represents the sensitivity experiment $S_{T\text{-}1}$, where temperature is decreased uniformly by 1 °C; the *dotted line* is the simulation S_{T+1}, where temperature is increased uniformly by 1 °C; the *dashed line* shows the carbon stock for $S_{T\pm1}$, where temperature is decreased in the NH and increased in the Southern Hemisphere by 1 °C. Atmospheric CO_2 concentrations are set to a preindustrial value of 281 ppm

---

For experiment $S_{T\pm1}$, all tree plant functional types show a southward shift in both hemispheres, where they find better growing conditions. The spatial coverages of the different PFTs at the new equilibrium (450 years after the temperature perturbation) in comparison to preindustrial conditions are plotted for individual latitudinal bands (Fig. 3). Tree coverage is decreasing at high northern latitudes where growing conditions get worse. The global area covered by vegetation is not changed significantly by the temperature perturbation as it is only 1.1% smaller after the changes in temperature. The global carbon stock is mainly influenced by the air temperature decrease in the NH, because the main part of land area is in the NH. The global terrestrial carbon inventory increases by 27 GtC. Terrestrial carbon storage increases in the southern part of boreal regions (USA and Eurasia) due to decreased soil respiration rates, whereas the storage decreases in high northern latitudes where tree coverage has decreased (Fig. 4).

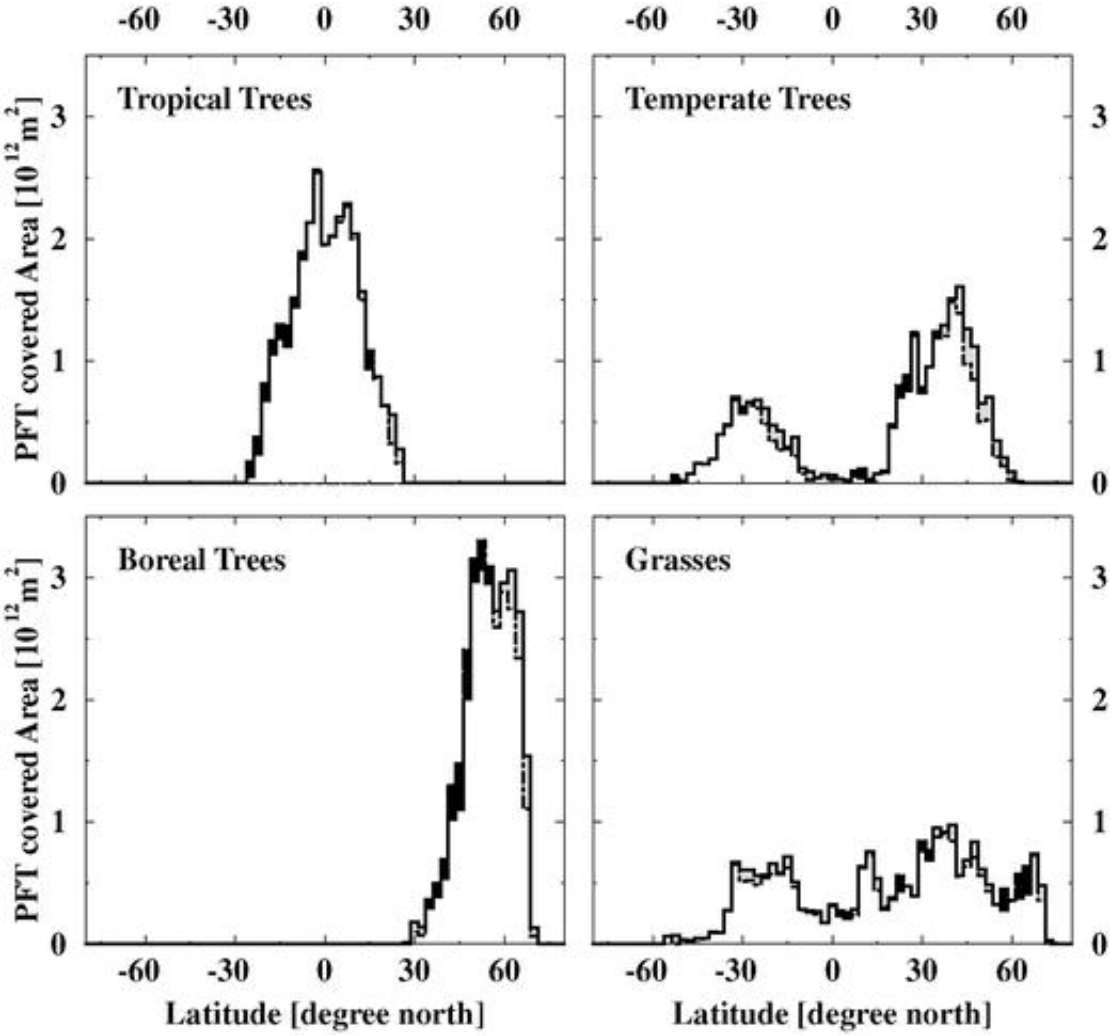

Fig. 3. Sensitivity of plant cover to temperature changes. Areas covered by tropical trees, temperate trees, boreal trees, and grasses, resulting from the temperature sensitivity experiment $S_{T\pm1}$. *Solid lines* indicate plant coverages before temperature steps, *dashed lines* show coverages in the new equilibrium after experiment $S_{T\pm1}$. The *black area* indicates an increase, the *gray area* a decrease in plant cover of the different plant types. Areas covered by plants (in m^2) are shown for latitudinal bands with a resolution of 2.5°

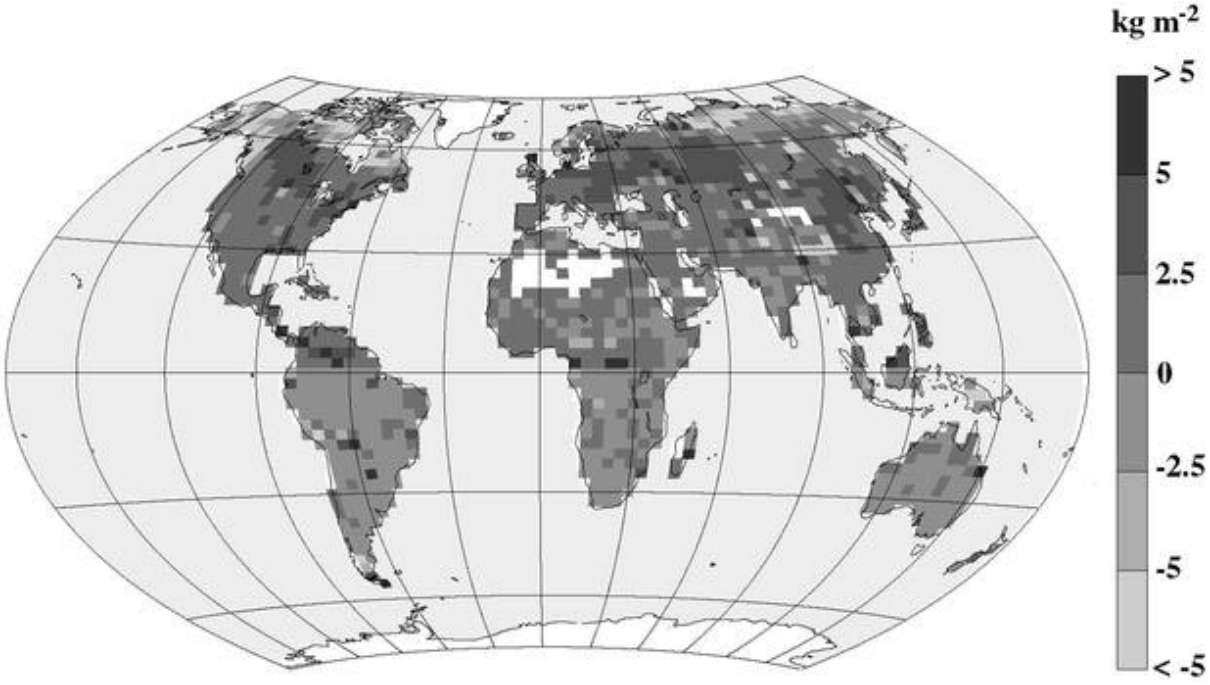

Fig. 4. Perturbations in the terrestrial carbon storage due to a step in air temperatures by -1 °C in the NH and, by +1 °C in the SH (experiment $S_{T\pm1}$). Carbon inventory changes are plotted 450 years after the temperature perturbation, when the LPJ-DGVM has equilibriated with the new temperatures

---

Next, we address the sensitivity of the LPJ-DGVM to changes in the seasonality of surface temperatures. Variations in monthly temperatures from the annual mean value are changed by +10% or -10% respectively for every individual grid cell (experiments S_{S+10} and S_{S-10}). The global carbon pool contents change by +22 GtC in the new equilibrium with a weaker temperature seasonality and by -66 GtC with a stronger seasonality. The terrestrial carbon inventory is more sensitive to increasing seasonality because temperature stress for most PFTs increases significantly when summer temperatures are increased. The biggest changes in vegetation resulting from variations in temperature seasonality can be observed in mid- to high-latitudes.

3.1.2

Precipitation

In order to examine the reaction of the model to variations in precipitation, local precipitation values are instantaneously increased or decreased by a fixed percentage number at every grid cell (Table 1). Carbon storage increases (decreases) by about 12 GtC for an increase (decrease) in local precipitation by 2%. The terrestrial carbon inventory shows a slightly stronger sensitivity to precipitation decreases than to increases.

According to Voss and Mikolajewicz (*2001*), global precipitation changes by about 2.4% for temperature variations of 1 °C, and Hulme et al. (*1998*) also estimated precipitation sensitivity to be 2.4%/°C for the anthropogenic climate perturbation. Applying the sensitivity derived from a uniform precipitation perturbation yields then an estimated decrease in terrestrial carbon storage of about 15 GtC caused by the precipitation change associated with a temperature decrease of 1 °C. This is small compared to the increase in carbon storage of 75 GtC caused by a uniform temperature perturbation of 1 °C. In reality precipitation changes are not spatially uniform, but changes may be of opposite sign in

different regions. The spatial precipitation and temperature patterns (EOFs) derived from the 4 ×

CO_2 simulation with the ECHAM3/LSG have been applied as boundary conditions for the LPJ-DGVM. Then, the sensitivity of global terrestrial carbon storage to precipitation changes is smaller by about a factor 2.5 than the sensitivity to corresponding temperature changes.

3.1.3

Atmospheric CO_2

The sensitivity of the LPJ-DGVM to variations in atmospheric CO_2 concentrations is examined by instantaneously changing CO_2 level after the model spin-up. Climate variables are kept constant. After a CO_2 decrease by 5 ppm (sensitivity experiment S_{C-5}), the terrestrial carbon storage decreases by 20 GtC in the new equilibrium (Table 1). If the atmospheric CO_2 concentration is increased by 5 ppm (S_{C+5}), the terrestrial carbon storage changes by 4.6 GtC ppm^{-1}, but this coefficient decreases for higher changes in CO_2. A step of 500 ppm leads to a terrestrial uptake of 2.44 GtC ppm^{-1}, a step of 1000 ppm results in 1.74 GtC ppm^{-1}. A doubling of atmospheric CO_2 concentrations results in an increase in terrestrial carbon inventory of approximately one third, and when the CO_2 concentration is tripled, the carbon stock is increased by 50% under a constant climate. Approximately half of the whole carbon increment under increased CO_2 concentrations is found in the vegetation pool, about one third in the slow organic matter pool, and the rest in the litter pools. The reason for the additional carbon storage is the "CO_2-fertilization"; both the photosynthesis rate and the water use efficiency increase under higher CO_2. The effects of elevated atmospheric CO_2 concentrations on vegetation structure are that trees tend to out-compete grass PFTs because of their dominant position in light and water competition, and that tropical raingreen trees are partly displaced by tropical evergreen trees because of an increased water use efficiency and soil water availability. In the coupled carbon cycle-climate system, CO_2 fertilization acts as a negative feedback on climate-induced variations in atmospheric CO_2; an increase (decrease) in atmospheric CO_2 is partly mitigated by an increased (decreased) terrestrial storage.

The experiments presented in Table 1 correspond to highly idealized situations and the response of the carbon cycle to a climate perturbation depends on the combined spatio-temporal evolution of all climate variables. Nevertheless, results of the various sensitivity experiments suggest that global terrestrial carbon storage is most sensitive to variations in NH temperature and that comparable variations in precipitation have a much smaller effect on global storage. Furthermore, additional simulations to those presented have revealed that cloud cover changes have a minor effect on modeled carbon storage and plant cover. The LPJ-DGVM shows a strong change in terrestrial carbon storage in response to changes in atmospheric CO_2 that tends to dampen any climate-induced fluctuation in atmospheric CO_2.

3.2

The adjustment time of atmospheric CO_2 and $\delta^{13}C$ to a perturbation in climate

Next, time scales in the coupled carbon cycle-climate system are explored to evaluate how fast atmospheric CO_2 responds to changes in radiative forcing and temperature. First, a step perturbation

of 1 W m^{-2} in external radiative forcing is applied in the Bern CC model, using the patterns derived from the ECHAM3/LSG model. The model is run for another 900 years after the step. Temperature, precipitation, and cloud cover change rapidly in the first few decades after the step, but the final equilibrium is approached very slowly (Fig. 5A). The simulated change in atmospheric CO_2 (Fig. 5B) increases radiative forcing by up to 15% above the prescribed 1 W m^{-2}. Accordingly, temperatures are higher when considering radiative forcing by CO_2 (Fig. 5A) compared to a simulation where radiative forcing is kept at 1 W m^{-2}. Atmospheric CO_2 follows the temperature rise to peak about 100 years after the step. The initial increase of about 8 ppm is caused by both a reduced CO_2 solubility in the ocean and a terrestrial carbon release. A large fraction of the carbon released by the land biosphere is eventually sequestered by the ocean. This causes atmospheric CO_2 to decrease in the following centuries.

Changes in climate and the carbon cycle also affect the carbon isotopic ratios. The $^{13}C:^{12}C$ ratio is usually given as deviation from a standard ratio in permil $\delta\,^{13}C$. Atmospheric $\delta\,^{13}C$ changes are primarily governed by the following processes. Sea surface warming tends to increase atmospheric $\delta\,^{13}C$. Release of ^{13}C-depleted carbon from the land biosphere tends to decrease atmospheric $\delta\,^{13}C$. The perturbation in atmospheric $\delta\,^{13}C$ caused by terrestrial carbon release is removed by exchange with the ocean and the biosphere on time scales from decades to centuries. The interplay of these processes causes atmospheric $\delta\,^{13}C$ to decrease by about 0.07 ‰ within the first few decades after the step. This initial perturbation in atmospheric $\delta\,^{13}C$ is to a large extent removed within 150 years after the step change in radiative forcing (Fig. 5C). Afterwards, atmospheric $\delta\,^{13}C$ continues to increase and slowly approaches a slightly (0.01 ‰) higher value than before applying the perturbation in radiative forcing due to ocean warming.

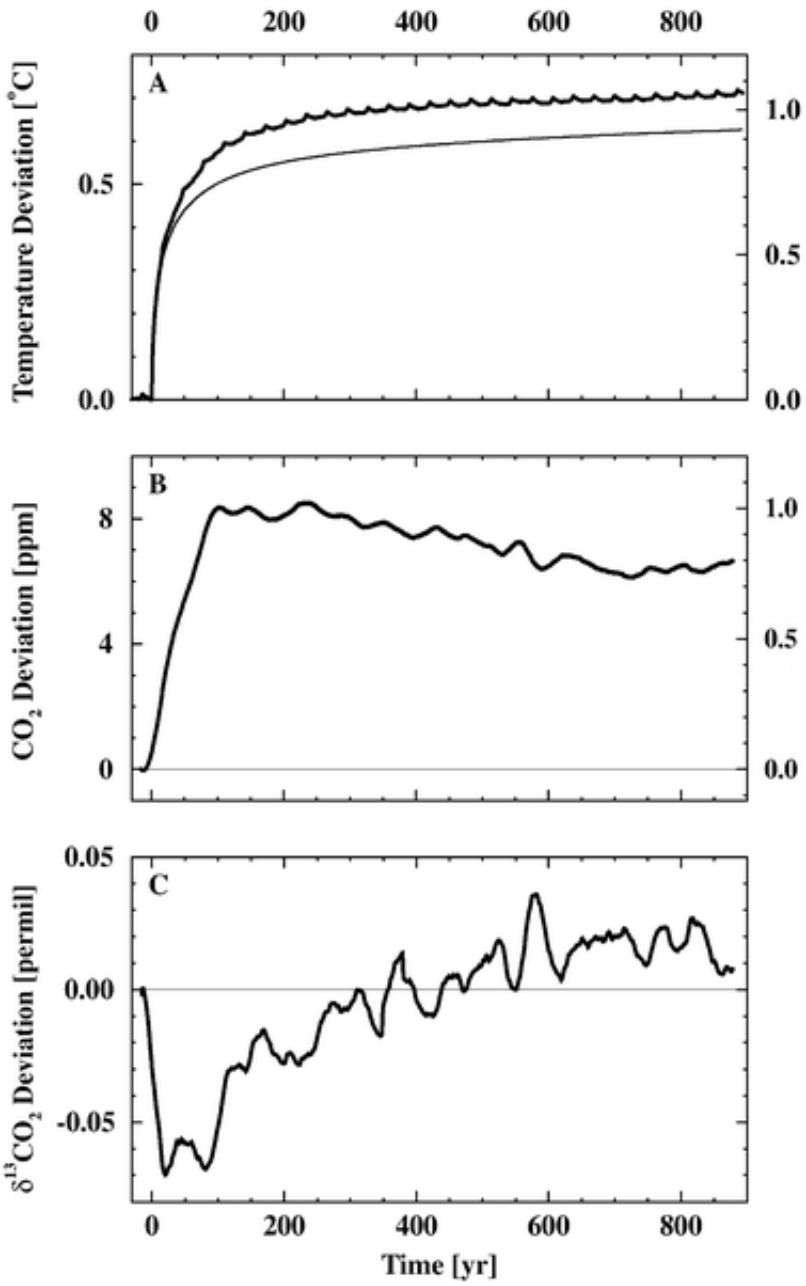

Fig. 5A-C. Timescales of the carbon cycle-climate system. The adjustment towards a new equilibrium is shown for **A** global mean surface temperature, **B** atmospheric CO_2, and **C** atmospheric $\delta^{13}C$ after a perturbation in radiative forcing. Radiative forcing due to solar irradiance has been increased by 1 W m^{-2} at time 0 and kept constant afterwards. Radiative forcing due to varying CO_2 has been calculated using a logarithmic relationship (Myhre et al. *1998*). The *right hand y-axis* in **A** indicates changes normalized to the equilibrium temperature change of 0.674 °C for a 1 W m^{-2} perturbation in total radiative forcing. The temperature evolution is also given for a simulation where radiative forcing by CO_2 is not considered (*thin solid line*). CO_2 and $\delta^{13}C$ results have been smoothed by 31-year running averages

Second, a step-like perturbation in temperature, precipitation, and cloud cover is applied that corresponds to the equilibrium climate change simulated by the ECHAM3/LSG IRF-EOF substitute for a change in radiative forcing of 1 W m^{-2}. Hence, changes in temperature, precipitation, and cloud cover are imposed instantaneously and kept constant thereafter, in contrast to the previous experiment where radiative forcing is changed instantaneously and the transient response in climate, atmospheric CO_2, and radiative forcing by CO_2 is simulated. Atmospheric CO_2 reacts rapidly to the perturbation and increases within 70 years by 10 ppm (Fig. 6). 63% ($1 - e^{-1}$) of this initial increase is achieved within 12 years. After peaking, atmospheric CO_2 decreases slowly in the following centuries. 63% of the peak perturbation in atmospheric $\delta^{13}C$ is removed by the ocean and the terrestrial biosphere within about 100 years. Although a large range of time scales governs the response of atmospheric CO_2 and $\delta^{13}C$ to a climatic perturbation, the major response is evident one to two decades after the perturbation. This time range is comparable or narrower than the typical width of the age distribution of air enclosed in an individual bubble in ice. The width of the age distribution is about 20 years for the cores drilled at Law Dome, a high accumulation site, and larger for the other cores. The important implication is that atmospheric CO_2 closely follows decadal-mean temperature changes if changes in ocean circulation and ocean-sediment interactions such as those responsible for the glacial-interglacial CO_2 variations are not important. In other words, changes in simulated atmospheric CO_2 under such conditions reflect to a large extent changes in simulated surface temperatures averaged over one to two decades.

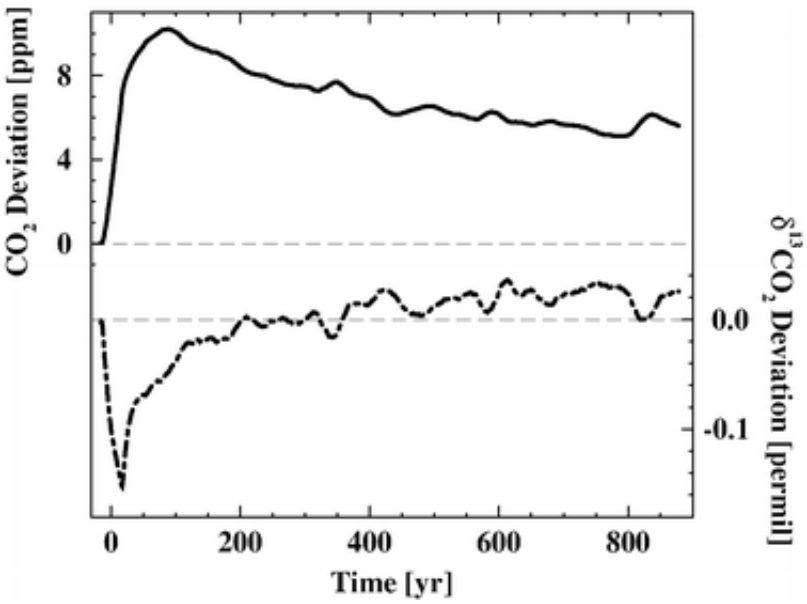

Fig. 6. The adjustment of atmospheric CO_2, and $\delta^{13}C$ after a step-like perturbation in climate. Global mean temperature has been increased by 0.674 °C at time zero and kept constant afterwards; perturbation fields of temperature, precipitation, and cloud cover from the ECHAM3/LSG model have been scaled accordingly. Results have been smoothed by 31-year running averages

---

3.3

The modeled evolution of atmospheric CO_2 and temperature over the last millennium in response to solar and volcanic forcing

In this section, we investigate whether NH mean surface temperature reconstructions and ice core CO_2 data are consistent within the framework of the Bern CC model, i.e., whether we are able to simulate the reconstructed evolution of atmospheric CO_2 and NH mean temperature (Fig. 1B, C) when the model is forced with reconstructed solar and volcanic forcing (Fig. 1A). Radiative forcing from solar irradiance changes and explosive volcanic eruptions are prescribed in the Bern CC model and the evolution of temperature, precipitation, cloud cover, atmospheric CO_2 and radiative forcing by CO_2 is simulated over the past millennium. Radiative forcing by other anthropogenic greenhouse gases and aerosols and anthropogenic carbon emissions are taken into account for the industrial period.

Calculated changes in NH mean surface temperatures and atmospheric CO_2 over the last millennium are broadly compatible with many of the observationally based records (Fig. 7) for the standard model setup and for a range of climate sensitivities (Table 2: simulations S1 to S3). High temperatures are simulated during the twelth century, whereas the lowest hemispheric mean surface temperatures of the millennium are simulated during the sixteenth and seventeenth centuries. The modeled preindustrial NH temperature varies within a range of 0.5 °C, within the uncertainty of various reconstructions (Briffa and Osborn *2002*). The modeled temperature range is comparable to the best estimate by Mann et al. (*1999*) in the standard simulation but larger than in this reconstruction for a simulation with a high climate sensitivity (Fig. 7). On the other hand, simulated temperature fluctuations are considerably less than suggested by Esper et al. (*2002*).

Table 2. Simulated temperature and CO_2 variations for different model setups

Simulation	ΔT_{2x}	NH ΔT(1480-1180)	ΔCO_2 (1480-1180)
Standard model setup (Fig. 7)			
Standard model configuration with coupled radiative forcing, climate, and carbon cycle modules; reconstructed solar and volcanic radiative forcing prescribed (Fig. 1A); variations in climate and atmospheric CO_2 calculated.			
(S1) Standard climate sensitivity	2.5 °C	0.42 °C	4.1 ppm
(S2) Low climate sensitivity	1.5 °C	0.30 °C	2.5 ppm
(S3) High climate sensitivity	4.5 °C	0.58 °C	6.8 ppm
Sensitivity experiments (Fig. 8)			
(S4) Radiative forcing by volcanoes omitted	2.5 °C	0.21 °C	2.8 ppm
(S5) Terrestrial carbon storage kept constant	2.5 °C	0.41 °C	2.3 ppm
(S6) Sea surface temperature kept constant	2.5 °C	0.41 °C	3.1 ppm
Suppressed terrestrial CO_2 fertilization			
(S7) Standard climate sensitivity	2.5 °C	0.44 °C	8.2 ppm
(S8) Low climate sensitivity	1.5 °C	0.36 °C	4.9 ppm
(S9) High climate sensitivity	4.5 °C	0.63 °C	11.0 ppm
Anthropogenic impact (Fig. 9)			
(S10) Anthropogenic emissions omitted	2.5 °C	0.42 °C	4.1 ppm
(S11) Pre-industrial land use emissions scaled to population growth	2.5 °C	0.41 °C	3.2 ppm
Variations in radiative forcing (Fig. 11)			
Solar radiative forcing is multiplied by a factor of 2.6 (Fig. 1A, thin line)			
(S12) Standard climate sensitivity	2.5 °C	0.74 °C	8.0 ppm
(S13) Low climate sensitivity	1.5 °C	0.53 °C	5.8 ppm
(S14) High climate sensitivity	4.5 °C	1.00 °C	10.9 ppm
(S15) Solar radiative forcing multiplied by a factor of 5	4.5 °C	1.65 °C	18.8 ppm

The climate sensitivity (ΔT_{2x}) applied in the simulations (S1) to (S15) is shown in the first data column. Simulated differences in NH mean surface temperature (NH ΔT) and atmospheric CO_2 (ΔCO_2) have been evaluated for the relative maximum around 1180 AD and the relative minimum around 1480 AD

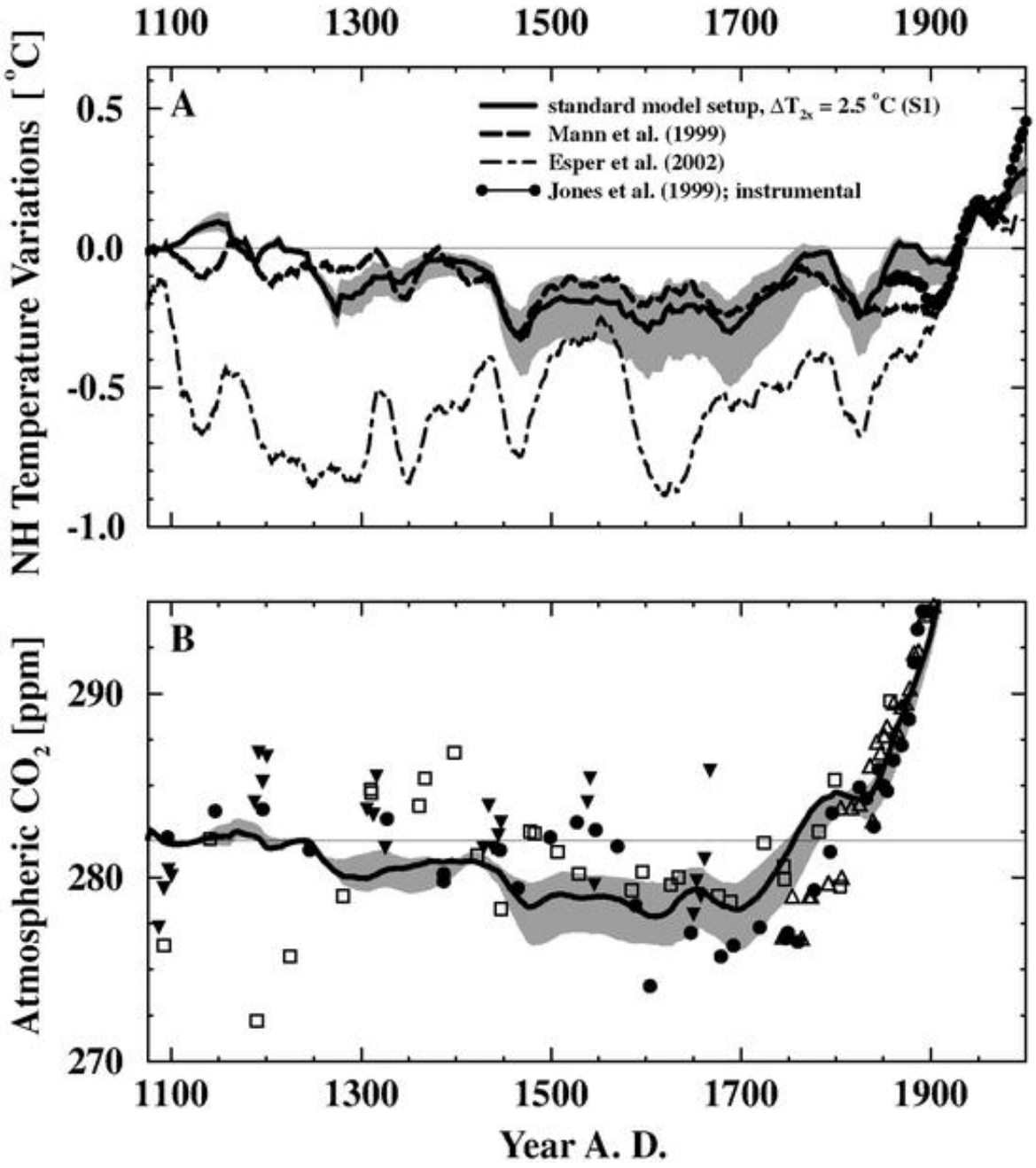

Fig. 7A, B. Modeled NH temperature and atmospheric CO_2 during the last millennium. **A** Simulated deviations in NH mean surface temperature and **B** atmospheric CO_2 when radiative forcing from solar irradiance changes (Fig. 1A, *top*, *thick solid* line and explosive volcanic eruptions (**A** *bottom*) is prescribed in the Bern CC model. The model's climate sensitivity is set to 2.5 °C in the standard simulation S1 (*solid*) and to 1.5 °C (S2) and 4.5 °C (S3) to obtain the *shaded band*. Reconstructed NH mean surface temperature by (Mann et al. *1999*) (*dashed line*), (Esper et al. *2002*) (*dot-dashed line*), the instrumental temperature record (*solid circles*), and the ice core CO_2 record (*symbols*) are shown for comparison. Results have been smoothed by 31-year running averages

The reconstruction by Esper et al. (*2002*) shows much larger amplitudes of the temperature variations than other comparable reconstructions (Briffa and Osborn *2002*). Reconstructed temperatures by Esper et al. (*2002*) are lower by about 0.3 °C than the instrumental record during the second half of the nineteenth century. The amplitude of the reconstructed temperature depends on the scaling (Briffa and Osborn *2002*). It is halved when the averaged unsmoothed regional curve standardization (RCS) data of Esper et al. (*2002*) (Esper personal communication) are scaled to the unsmoothed instrumental record (NH annual mean, land and ocean) over the period 1852 to 1993 as compared to scaling the smoothed data over the period 1900 to 1977 only, as done by Esper et al. (*2002*). Such a rescaling would bring the amplitudes of the RCS data-based reconstruction in better agreement with the modeled temperature fluctuations and with the amplitudes of other empirical reconstructions. Individual minima and maxima in modeled temperature are reflected in the different temperature reconstructions (Mann et al. *1999*; Esper et al. *2002*; Briffa and Osborn *2002*) (Fig. 7). For example, the minimum around 1475 and the maxima around 1550 and 1775 are consistently found in the model results and the reconstructions by Esper et al. (*2002*) and Mann et al. (*1999*). Simulated temperature increases after a minimum in solar and volcanic forcing between 1825 and 1865 similar to the reconstruction by Esper et al. (*2002*) whereas the reconstruction by Mann et al. (*1999*) shows little change during this period. On the other hand, minima and maxima of the temperature reconstructions and the model results are to a large degree out-of-phase during the early part of the millennium.

The modeled global mean surface temperature increase over the twentieth century is 0.39 °C, comparable to the estimate of 0.6 ± 0.2 °C derived from instrumental data (Folland et al. *2001*), for the standard simulation S1 in which the climate sensitivity is set to 2.5 °C. The lower than observed surface temperature increase modeled for the twentieth century may be due to an overestimation of the cooling effect by anthropogenic aerosols (Knutti et al. *2002*) in combination with a relatively low climate sensitivity.

Modeled atmospheric CO_2 varies within a range of 5 ppm before the onset of industrialization in the standard simulation S1, well within the scatter of the ice core data (Fig. 7B). Simulated CO_2 decreases after 1180 to reach a first minimum around 1480. Concentrations remain low during the sixteenth and seventeenth centuries. Atmospheric CO_2 increases rapidly during the industrial period due to anthropogenic carbon emissions.

In summary, simulated changes in atmospheric CO_2 and NH mean surface temperature are broadly compatible with the ice core CO_2 data and with temperature reconstructions.

3.4

Sensitivity of NH temperature and atmospheric CO_2 to forcings and carbon cycle processes

The importance of individual mechanisms and forcings for the modeled changes in climate and CO_2 is investigated (simulations S4 to S9, Fig. 8).

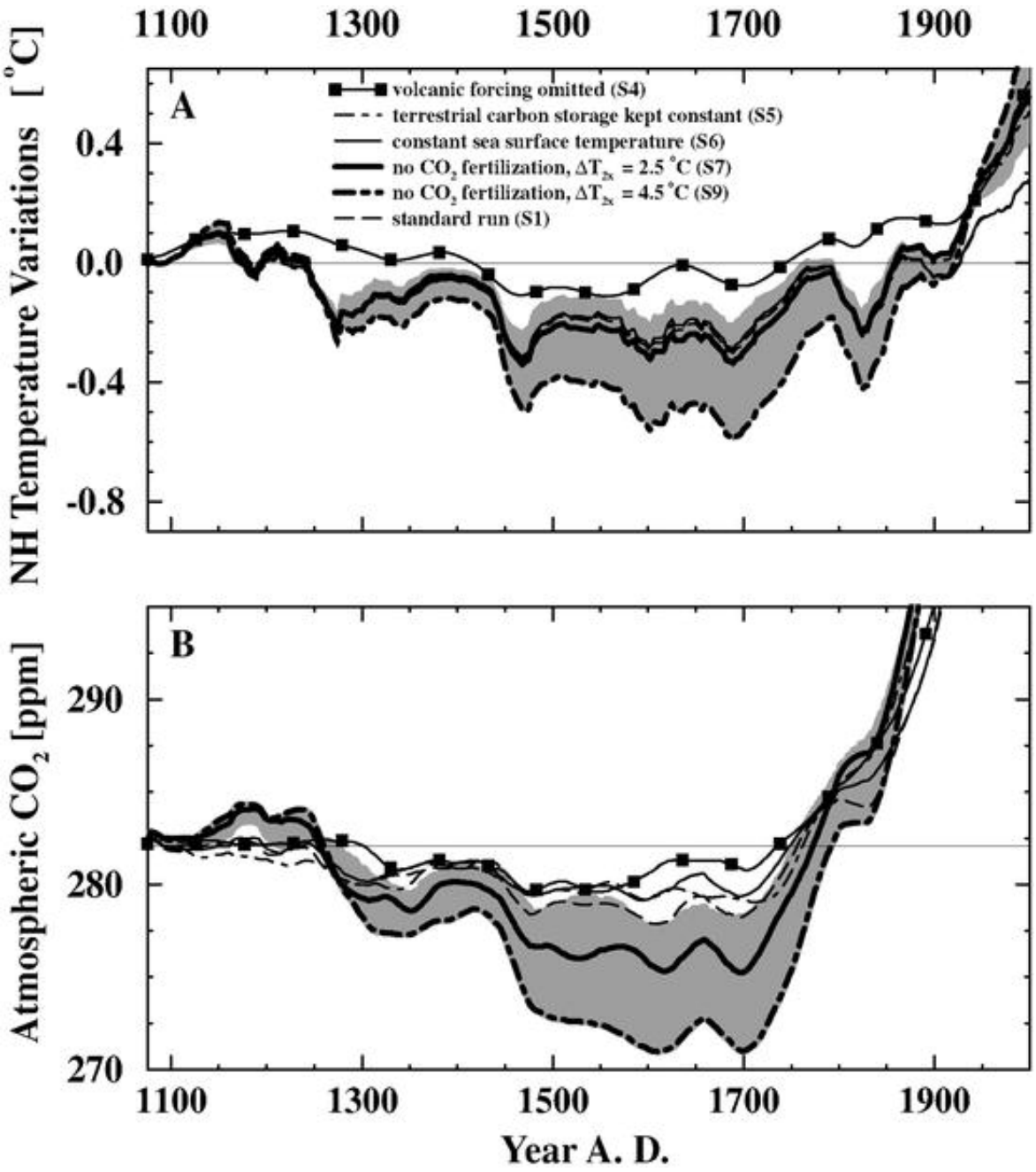

Fig. 8A, B. Sensitivity of NH temperature and atmospheric CO_2 to volcanic forcing and carbon cycle processes. **A** Simulated deviations in NH mean surface temperature and **B** atmospheric CO_2 for different sensitivity experiments in which volcanic forcing is excluded (S4, *solid squares*), terrestrial changes are excluded (S5, *thin, dot-dashed*), ocean surface temperature is kept constant (S6, *thin, solid*), while all other parameters and input data are as in the standard simulation (S1, *dashed*). In another set of simulations, CO_2 fertilization is suppressed (*thick solid line*) and ΔT_{2x} varied between 1.5 °C and 4.5 °C (*thick, dot-dashed*) to obtain the gray band (S7 to S9). Results have been smoothed

Volcanic forcing contributes substantially to the low temperatures and low CO_2 values during the sixteenth and seventeenth centuries. Atmospheric CO_2 decreases by 2.8 ppm between 1180 and 1480 AD in simulation S4, where volcanic forcing is excluded, compared to 4.1 ppm in S1. In S4, simulated NH mean surface temperature and atmospheric CO_2 start to increase already around 1550.

The CO_2 decrease during the first half of the millennium results from both an increase in global terrestrial carbon storage and an increase in the CO_2 solubility in ocean surface waters in response to cooling. Atmospheric CO_2 decreases by 2.3 ppm between 1180 AD and 1480 AD in simulation S5 where terrestrial carbon storage is kept constant. In simulation S6 where the ocean surface temperature is kept constant, the reduction in atmospheric CO_2 is 3.1 ppm between 1180 and 1480 AD.

Terrestrial CO_2 fertilization acts as a strong feedback mechanism on atmospheric CO_2 variations. In simulations S7 to S9 (ΔT_{2x} = 1.5; 2.5; 4.5 °C) terrestrial CO_2 fertilization is suppressed by prescribing a constant CO_2 concentration in the model's photosynthesis module. Then, the modeled atmospheric CO_2 decrease is about 80% larger than for the standard model setup. The decrease in CO_2 is 11 ppm (1180-1480 AD) and the simulated range in NH mean surface temperature is 0.6 °C for simulation S9 where a high climate sensitivity is applied. The amplitude of the simulated atmospheric CO_2 variations may still be consistent with the ice core CO_2 data and their uncertainties.

Anthropogenic emissions and forcings are excluded in simulation S10 to investigate forced natural variability over the industrial period. Simulated temperatures remain low and NH mean surface temperature is decreasing over the past few decades (Fig. 9A). Externally forced natural climate variations have contributed by a few ppm to the early rise in atmospheric CO_2 in the eighteenth century, but simulated concentrations remain below 282 ppm until year 2000.

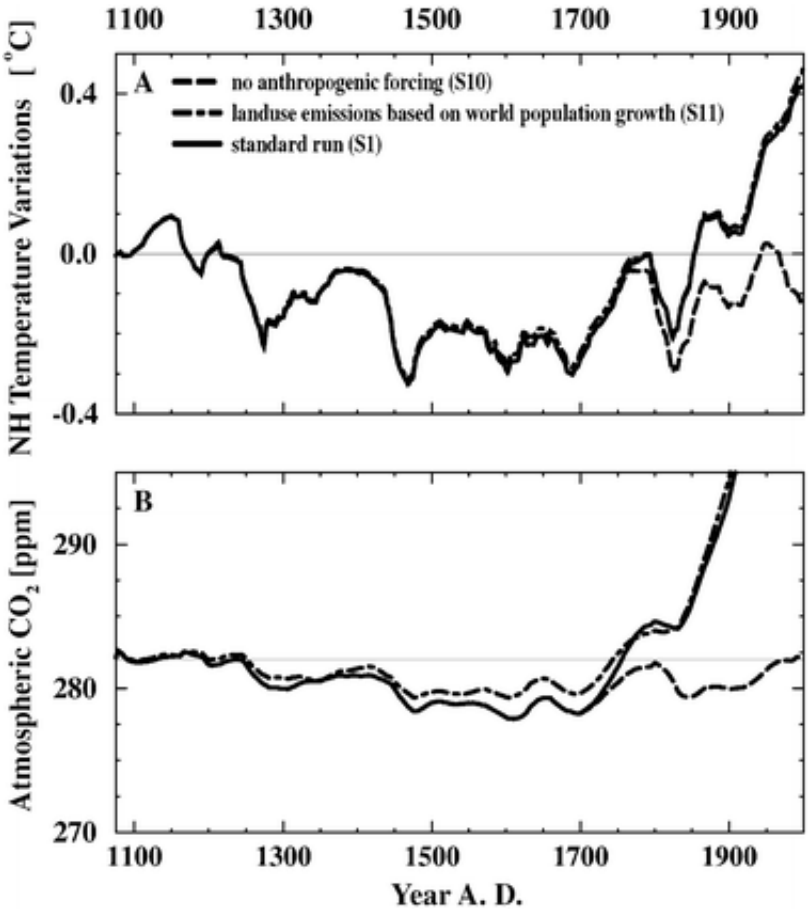

Fig. 9A, B. The anthropogenic impact on NH temperature and CO_2. **A** Simulated deviations in NH mean surface temperature and **B** atmospheric CO_2 for different sensitivity experiments in which anthropogenic emissions are excluded (S10, *dashed*), land use emissions are scaled to population growth prior to 1850 (S11, *dot-dashed*). All results have been smoothed. Results of the standard simulation (S1, *solid*) are shown for comparison

---

Next, an alternative scenario for land use emission is explored. Land use emission data are available back to 1850 (Houghton *1999*) and these data are prescribed in the model. Prior to 1850, land use emissions between 1700 and 1850 have been obtained by linear interpolation assuming zero emission up to year 1700 in the standard model setup. In simulation S11, land use emissions are scaled to population growth prior to 1850. This is done by first estimating carbon emissions per increase in population. Between 1850 and 1990 122 GtC were emitted by land use (Houghton *1999*) and population increased by 4.024 billion (United Nations *1999*). This yields a factor of 0.03039 (GtC yr^{-1})/(million yr^{-1}). This factor is multiplied with population growth rate computed from the United Nations (*1999*) population data to obtain land use emissions prior to 1850. Population increased from 310 million to 1260 million between 1000 AD and 1850 AD. This yields cumulative land use emissions of 36 GtC from the begin of the simulation at 1075 up to 1850 or roughly 23% of the total emissions between 1075 and 1990. This compares well with the finding that an area equivalent to 24% of the total area cultivated at year 1990 has been cultivated at year 1850 (Houghton *1999*). Simulated temperatures are hardly discernible between simulation S11 and the standard simulation S1 (Fig. 9A). Atmospheric CO_2 is only slightly higher in simulation S11 than in the standard simulation prior to 1800 (Fig. 9B). This suggests that assumptions about land use emissions

are not critical for this study.

Changes in terrestrial carbon storage vary considerably over the globe (Fig. 10). The simulated cooling during the first half of the millennium leads to an increased global terrestrial storage of about 12 GtC by 1700 AD in the standard simulation S1. Totals of 15 GtC are taken up by vegetation and soils in low and mid northern latitudes (0-60°N), whereas only about 5 GtC is sequestered in the SH. By 1700, about 9 GtC have been lost to the atmosphere in high northern latitudes (>60°N) due to less favorable growth conditions in these temperature stressed areas. This loss tends to partly offset the carbon gain at other latitudes. The CO_2 fertilization mechanism is most effective in northern mid-latitudes and between 0 to 30°S. About 28 GtC are sequestered globally by 1700 AD in simulation S7 where CO_2 fertilization is suppressed. This is more than twice than in the standard case.

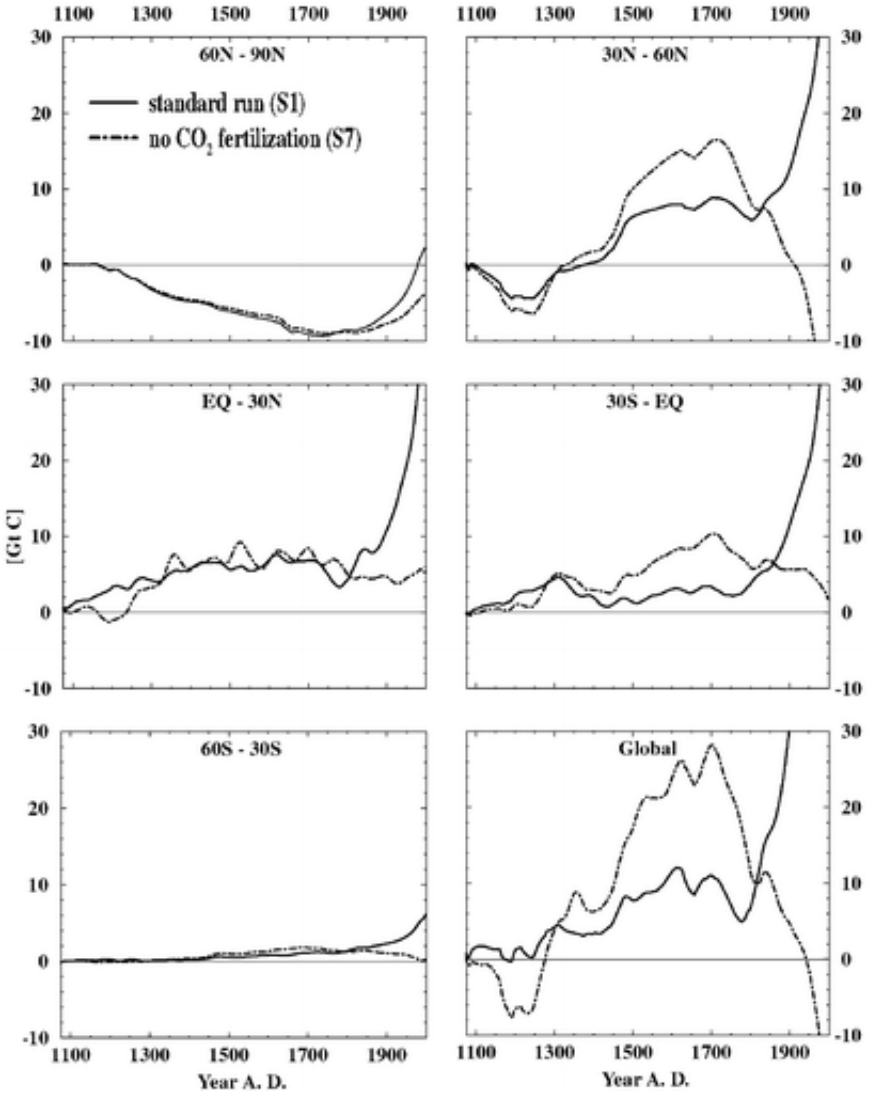

Fig. 10. Perturbation in terrestrial carbon storage for different latitudinal bands in GtC for the standard simulation (S1, *thick solid*) and for simulation S7 where terrestrial CO_2 fertilization is suppressed (*dot-dashed*). ΔT_{2x} is 2.5 °C in both simulations. Results are smoothed by a 31-year running average. Area covered by land is $1.36 \cdot 10^{13}$ m^2 (60°N-90°N), $4.69 \cdot 10^{13}$ m^2 (30°N-60°N), $3.85 \cdot 10^{13}$ m^2 (Equator - 30°N), $2.84 \cdot 10^{13}$ m^2 (30°S - Equator), and $6.20 \cdot 10^{12}$ m^2 (60°S-30°S)

No individual forcing factor or process of the carbon cycle can explain the modeled evolution of climate and atmospheric CO_2 alone; the modeled evolution is rather determined by the interplay of a variety of forcings and processes. Our results suggest that atmospheric CO_2 would have remained around the preindustrial level of 280 ppm without anthropogenic emissions.

3.5

Constraining past temperature variations by the ice core CO_2 record

Next, the magnitude of past variations in NH surface temperature is constrained by requiring modeled CO_2 to be within the range of the ice core CO_2 data. We will restrict major parts of our analysis to the period before 1700 as anthropogenic emissions are not well known for the early industrial period. Solar forcing and the model's climate sensitivity ΔT_{2x} was varied to explore atmospheric CO_2 changes for a range of variations in NH mean surface temperature and climate (S12 to S15, Fig. 11). The difference between the warmest and coldest preindustrial temperatures increases from 0.4 °C in the standard simulation S1, to 1.0 °C in simulation S14 where climate sensitivity is higher (ΔT_{2x} = 4.5 °C) and solar irradiance multiplied by a factor of 2.6, corresponding to the upper bound of recent reconstructions (Bard et al. *2000*; Reid *1997*) (Fig. 1A, thin line). The variation in preindustrial CO_2 is 5 ppm and 12 ppm, respectively. To mimic a high solar forcing variability and a high amplification of solar forcing in the climate system, solar irradiance changes in simulation S15 are assumed to be five times larger than in the standard simulation S1. Then, the simulated preindustrial temperature and CO_2 variations are further increased to 1.7 °C and 20 ppm, respectively. A variation in atmospheric CO_2 of 20 ppm clearly exceeds any variations in the ice core CO_2 data and implies that this high solar forcing scenario is unrealistic.

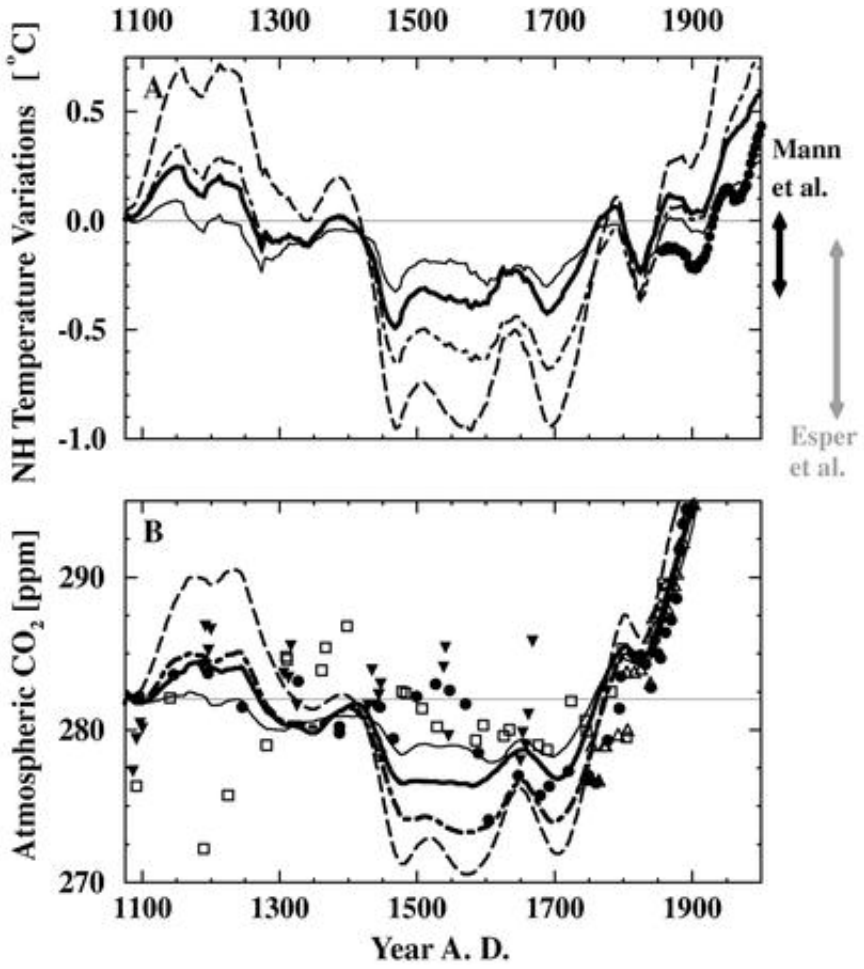

Fig. 11A, B. Sensitivity of NH temperature and CO_2 to changes in solar irradiance. **A** Simulated deviations in NH mean surface temperature and **B** atmospheric CO_2 applying different ΔT_{2x} and different scaling factors for total solar irradiance (31-yr running average). Solar forcing used in S1 (*thin, solid*) *line* is multiplied by 2.6 (0.65% reduction during the Maunder Minimum, *thin solid line* in Fig. 1) and ΔT_{2x} is set to 2.5 °C (S12, *thick, solid*) *line* and 4.5 °C (S14, *thick, dot-dashed*). Solar forcing is multiplied by a factor of five and ΔT_{2x} is set to 4.5 °C (S15, *long-dash*) to explore the impact of a high solar climate forcing. The instrumental temperature record (*solid circles*), the preindustrial range (1075-1700) for the Mann et al. (*1999*), Esper et al. (*2002*) reconstructions (*arrows*) and the ice core CO_2 record (*symbols*) are shown for comparison

---

We tentatively estimate a quantitative upper limit of preindustrial multi-decadal NH temperature variations by combining ice core data and model results. First, we establish the relationship between changes in NH temperature and changes in atmospheric CO_2 for the standard model setup and a range of climate sensitivities and solar irradiance changes by calculating regression coefficients between deviations in NH mean surface temperature versus deviations in atmospheric CO_2 for the simulations S1 to S3 and S12 to S15. Annual data are smoothed by a 21 year running average. The 21 year smoothing is motivated by the results of the step experiments described in Sect. 3.2 and by the width of the age distribution of air enclosed in ice. Linear regression of these smoothed data yields a slope, α, of 0.080 ± 0.0003 °C ppm^{-1} (r = 0.97). A value of 0.08 °C ppm^{-1} for α corresponds to a CO_2 change of 12 ppm caused by a change in NH temperature of 1 °C, and to a change of about 15 ppm for

a change in global surface temperature of 1 °C. Second, for consistency with the CO_2 record we request that CO_2 variations are within four standard deviations, i.e. 12 ppm, of the CO_2 data (1100 to 1700 AD). It follows that NH mean surface temperature must have varied within a range of 1 °C ($\alpha \times$ 12 ppm) between 1100 and 1700 AD. The effect of model uncertainties is investigated by repeating the same analysis for two extreme cases. Simulations S7 to S9 where CO_2 fertilization is completely suppressed yield a 46% smaller α (α = 0.0428 ± 0.0004 °C ppm^{-1}, r = 0.92), whereas simulations where ocean surface warming only contributes to atmospheric CO_2 variability (S5, plus additional simulations with different scaling of solar forcing and different climate sensitivities) yield a value for α twice as large as for simulations S1 to S3 and S12 to S15) (α = 0.1565 ± 0.0007 °C ppm^{-1}, r = 0.96). This suggests that the estimated upper limit for preindustrial, multi-decadal NH temperature variations of 1 °C is uncertain by up to a factor of two due to carbon cycle model uncertainties.

In conclusion, simulations where the magnitude of solar irradiance changes is increased yield a mismatch between model results and CO_2 data, providing evidence for modest changes in solar irradiance and global mean temperatures over the past millennium and arguing against a significant amplification of the response of global or hemispheric annual mean temperature to solar forcing. An increase in modeled NH or global mean surface temperature of 1 °C causes atmospheric CO_2 to rise by 12 ppm or 15 ppm, respectively. The model simulations therefore suggest that NH mean surface temperature changes between 1100 and 1700 AD were less than 1 °C to maintain atmospheric CO_2 changes within the data range of 12 ppm.

3.6

Atmospheric $\delta^{13}C$

The atmospheric ratio of the stable carbon isotopes ^{13}C to ^{12}C has the potential to provide additional information on past carbon cycle and climate variations (e.g., Indermühle et al. *1999*). Net terrestrial carbon uptake results in an increase in atmospheric $\delta^{13}C$, because the light isotope ^{12}C is preferentially assimilated by plants. Atmospheric $\delta^{13}C$ is also altered in response to changes in sea surface temperature, changes in the distribution of C_3 versus C_4 plants, and by changes in temperature, precipitation and CO_2 that alter the stomatal conductance. Changes in the marine biological cycle could also affect $\delta^{13}C$, but are not simulated in our model. Only ice core data from Law Dome, Antarctica, are available to us for the period 1000 AD to 1700 AD. The Law Dome $\delta^{13}C$ data (Francey et al. *1999*) suggest that $\delta^{13}C$ remained almost constant during the first part of the millennium. Measured values are up to 0.1‰ higher during the eighteenth than during the sixteenth century (Fig. 12). This has been interpreted as an indication of an increased terrestrial storage in response to cool temperatures (Trudinger et al. *1999*; Joos et al. *1999a*). However, the discrepancies between the Law Dome data and other recent state-of-the-art measurements on ice from Dome Fuji, Antarctica, (Kawamura et al. *2000*) suggest that small $\delta^{13}C$ variations must be interpreted with caution.

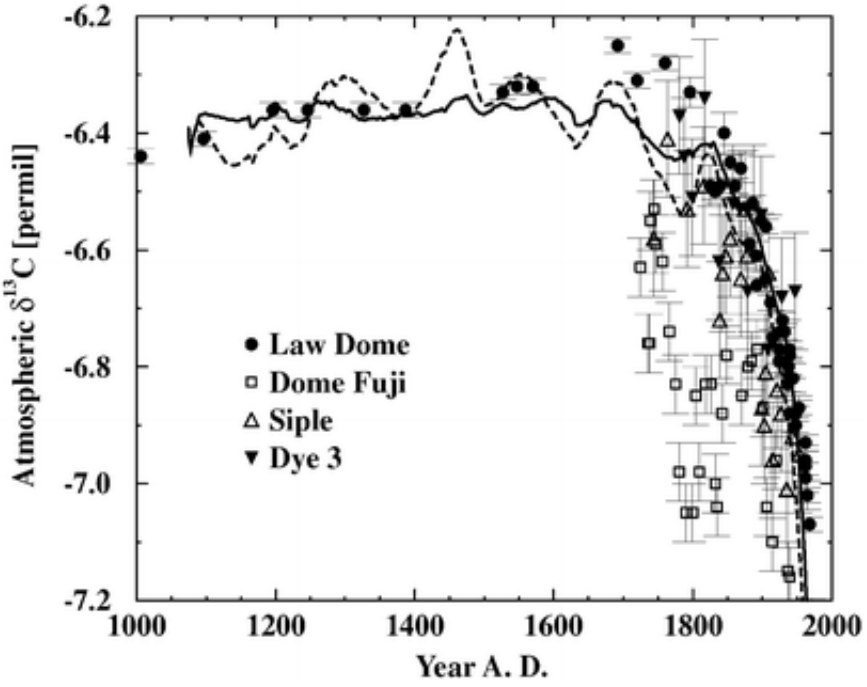

Fig. 12. Measured versus modeled atmospheric δ^{13}**C**. Measured δ^{13}C (permil) values are from air entrapped in ice drilled at Law Dome (Francey et al. *1999*), Siple Station (Friedli et al. *1986*), Dye 3 (Leuenberger *1992*) and Dome Fuji (Kawamura et al. *2000*) and model results from the standard simulation S1 (*solid*) and simulation S15 where solar forcing is multiplied by a factor of five and ΔT_{2x} set to 4.5 °C (*dashed*). Results have been smoothed

---

Simulated preindustrial atmospheric δ^{13}C variations (31-year average) are smaller than 0.05‰ in the standard simulation (S1) and less than 0.25‰ in simulation S15, with a high climate sensitivity and extreme solar forcing (Fig. 12). Simulated and reconstructed δ^{13}C decrease rapidly during the industrial period due to the input of ^{13}C depleted CO_2 from fossil fuel burning and land use emissions. We conclude that available δ^{13}C ice core data do currently not allow us to further constrain past variations in NH temperature.

4

Conclusion and discussion

In this study, we have evaluated the response of the Bern CC model by comparing simulated with reconstructed variations in NH mean surface temperature and atmospheric CO_2 over the last millennium. We find reasonable compatibility between simulated and reconstructed variations in temperature and atmospheric CO_2 given the uncertainties in the reconstructions and in reconstructed radiative forcing that is used as input in our model.

An implicit assumption in our modeling approach is that past, externally forced, low-frequency variations in temperature and precipitation have the same regional patterns as obtained for anthropogenic greenhouse gas forcing. Regional changes in temperature and precipitation have been

calculated by scaling the computed evolution of global mean temperature changes with time-invariant patterns derived from a GHG-only experiment with the ECHAM3/LSG. Spatial dissimilarities between the climatic responses to increased solar forcing and increased CO_2 are found regionally in AOGCM simulations (Marshall et al. *1994*). However, Cubasch et al. (*2001*) report that the spatial patterns found in global warming simulations with and without direct sulfate aerosol forcing obtained with the same AOGCM are more similar to each other than to the patterns obtained by other AOGCMs. This indicates that the individual response characteristics of the various AOGCMs are dominating the response pattern rather than differences in the forcing. Marshall et al. (*1994*) and Cubasch et al. (*1997*) found in AOGCM simulations forced by reconstructed irradiance changes temperature variations in both hemispheres to be in phase and a temperature pattern similar to that obtained in simulations with changing CO_2 only. Cubasch et al. (*1997*) and Shindell et al. (*2001*) both report an enhanced temperature contrast between land and ocean with warming over the continents and large parts of the globe and cooling over some parts of the North Atlantic and North Pacific under increased solar irradiance, roughly consistent with the pattern associated with CO_2 forcing. Different climate models yield different regional changes in temperature and precipitation, which could imply important differences in the response of the terrestrial biosphere to global climate change. Leemans et al. (*2002*) found differences of less than 2% in simulated atmospheric CO_2 when applying temperature and precipitation patterns from four different AOGCMs in emission scenarios.

Changes in the thermohaline circulation are not considered in our model. Bond et al. (*2001*) suggest based on proxy data that reduced solar irradiance leads to a reduced formation rate of North Atlantic Deep Water (NADW) and less heat transport into the North Atlantic region. The modeling study of Delworth and Dixon (*2000*) demonstrates that moderate changes in the thermohaline circulation, as inferred by Bond et al. (*2001*), could be driven by changes in the state of the Arctic Oscillation. The negative Arctic Oscillation anomaly found by Shindell et al. (*2001*) during cold phases in their model is then consistent with a moderate reduction in the NADW formation rate suggested by Bond et al. (*2001*). A moderate reduction in NADW formation implies additional moderate cooling in the North Atlantic region and a hardly detectable warming in the SH (Stocker *1998*; Marchal et al. *1999a*). More clearly, Broecker (*2001*) argues that the "Medieval Warm Period" and the "Little Ice Age" primarily reflect changes in the thermohaline circulation and that temperatures varied in opposite direction in the NH and SH. However, evidence from ocean sediment cores for a significant variability in the ocean thermohaline circulation during the past millennium as well as evidence for an anti-phase relationship between temperature variations in the NH and SH remain ambiguous or even contradictory (Keigwin and Boyle *2000*; Bradley et al. *2001*; Hendy et al. *2002*). Earlier ocean model results (Joos et al. *1999b*; Marchal et al. *1999b*; Plattner et al. *2001*) suggest, in agreement with ice core CO_2 results, (Stauffer et al. *1998*; Marchal et al. *1999b*) that even strong changes in NADW formation have a small influence on atmospheric CO_2 on decadal-to-centennial time scales. Furthermore, simulations with a zonally averaged dynamical ocean model coupled to energy- and moisture-balance model of the atmosphere yield little changes in atmospheric CO_2 and NADW over the last millennium when driven with reconstructed forcing (Plattner et al. *2002*).

The ice core record of atmospheric CO_2 has been used to constrain the magnitude of natural low-frequency temperature variability during the last millennium. Our results are in agreement with reconstructions that suggest modest variations in NH mean temperature. Our results are neither compatible with large changes in solar irradiance nor with a strong amplification of solar forcing by feedbacks within the climate system such as enhanced cloud formation (Svensmark and Friis-Christensen *1997*). This supports earlier findings that solar variability has contributed relatively little to the observed twentieth century warming and that most of the twentieth century warming is due to anthropogenic forcing (Mitchell et al. *2001*).

A quantitative upper bound for natural low-frequency temperature variations during the last millennium has been estimated by requiring that simulated atmospheric CO_2 changes are not larger than four times the standard deviation of the ice core data. This is a conservative criterion as a significant part of the scatter in the CO_2 data shown in Fig. 1C probably reflects analytical problems. For example, recent measurements on remaining ice from the South Pole core show a largely reduced variability (Siegenthaler *2002*). This suggests that the current ice core record can be improved significantly. We propose that a new core be analyzed from a site with low temperatures, a relatively high accumulation, low deposition rates of carbonates and other impurities, and low levels of oxidants such as H_2O_2 (Tschumi and Stauffer *2000*) to obtain a high resolution CO_2 record over the last millennium.

The quantification of past temperature variations using the ice core record depends critically on the applied model. Here, we have used a simplified carbon cycle - climate model. This has allowed us to perform many simulations and to explore systematically the sensitivities and time scales of the coupled climate-carbon cycle model. It also yields clearly defined climatic perturbations to drive the carbon cycle model component. However, the model includes simplifications and important processes may not, or not adequately, be described. For example, internal, unforced climate variability has not been considered. Similarly, simulated terrestrial carbon uptake (release) differs between different DGVMs for a particular climate forcing. Key simulations of this study should be repeated using other carbon cycle-climate models including comprehensive models (Cox et al. *2000*; Friedlingstein et al. *2000*).

Acknowledgements. This work was supported by the Swiss National Science Foundation and the Electric Power Research Institute, Palo Alto, Ca. We thank Thomas Crowley for providing radiative forcing data, Jan Esper for providing his RCS tree ring data, Kasper Plattner for making available results of his millennium simulation, Jakob Schwander for a revised age-scale of the South Pole ice core, Urs Siegenthaler for sharing his preliminary CO_2 measurements, and the Lund-Potsdam-Jena Model group for many stimulating discussions and for making the LPJ-DGVM available.

References

Anklin M, Barnola JM, Schwander J, Stauffer B, Raynaud D (1995) Processes affecting the CO_2 concentration measured in Greenland ice. Tellus Ser B 47: 461-470

Bard E, Raisbeck G, Yiou F, Jouzel J (2000) Solar irradiance during the last 1200 years based on cosmogenic nuclides. Tellus 52 Ser B: 985-992

Barnola JM, Anklin M, Procheron J, Raynaud D, Schwander J, Stauffer B (1995) CO_2 evolution during the last millennium as recorded by Antarctic and Greenland ice. Tellus Ser B 47: 264-272

Beer J, Joos F, Lukasczyk C, Mende W, Rodriguez J, Siegenthaler U, Stellmacher R (1994) ^{10}Be as an indicator of solar variability and climate. In: Nesme-Ribes E (ed) The solar engine and its influence on terrestrial atmosphere and climate, Springer, Heidelberg, Berlin New York, pp 221-223

Bertrand C, Loutre MF, Crucifix M (2002) Climate of the last millennium: a sensitivity study. Tellus 54 Ser A: 221-224

Bigler MD, Wagenbach D, Fischer H, Kipfstuhl S, Miller H, Sommer S, Stauffer B (2002) Sulphate record from a northeast Greenland ice core over the last 1200 years based on continuous flow analysis. Ann Glaciol (in press)

Bond G, Kromer B, Beer J, Muscheler R, Evans MN, Showers W, Hoffmann S, Lotti-Bond R, Hajdas I, Bonani G (2001) Persistent solar influence on North Atlantic climate during the Holocene. Science 294: 2130-2136

Bradley RS, Briffa KR, Crowley TJ, Hughes MK, Jones PD, Mann ME (2001) The scope of Medieval warming. Science 292: 211-212

Briffa KR (2000) Annual climate variability in the Holocene: interpreting the message of ancient trees. Quat Sci Rev 19: 87-105

Briffa KR, Jones PD, Schweingruber FH, Osborn TJ (1998) Influence of volcanic eruptions on Northern Hemisphere summer temperature over the past 600 years. Nature 393: 450-455

Briffa KR, Osborn TJ (2002) Blowing hot and cold. Science 295: 22-27

Broecker WS (2001) Was the Medieval Warm Period global? Science 291: 1497-1499

Collatz GJ, Ribas-Carbo M, Berry JA (1992) A coupled photosynthesis - stomatal conductance model for leaves of C_4 plants. Aust J Plant Physiol 19: 519-538

Cox P, Betts R, Jones C, Spall S, Totterdell I (2000) Acceleration of global warming due to carbon cycle feedbacks in a coupled climate model. Nature 408: 184-187

Cramer W, Bondeau A, Woodward FI, Prentice IC, Betts RA, Brovkin V, Cox PM, Fisher V, Foley JA, Friend AD, Kucharik C, Lomas MR, Ramankutty N, Sitch S, Smith B, White A, Young-Molling C (2001) Global response of terrestrial ecosystem structure and function to CO_2 and climate change: results from six dynamic global vegetation models. Global Change Biol 7: 357-373

Crowley TJ (2000) Causes of climate change of the last 1000 years. Science 289: 270-277

Crowley TJ, Lowery T (2000) How warm was the Medieval warm period? Ambio 29: 51-54

Cubasch U, Meehl GA, Boer GJ, Stouffer RJ, Dix M, Noda A, Senior CA, Raper S, Yap KS (2001) Projections of future climate change. In: Houghton JT, Ding Y, Griggs D, Noguer M, van der Linden P, Dai X, Maskell K, Johnson CA (eds) Climate change 2001: The scientific basis. Contribution of Working Group I to the Third Assessment Report of the Intergovernmental Panel on Climate change, Cambridge University Press, Cambridge, United Kingdom pp 525-582

Cubasch UR, Voss R, Hegerl GC, Waszkewitz J, Crowley TJ (1997) Simulation of the influence of solar radiation variations on the global climate with an ocean-atmosphere general circulation model. Clim Dyn 13: 757-767

Delworth TL, Dixon KW (2000) Implications of the recent trend in the Arctic/North Atlantic Oscillation for the North Atlantic thermohaline circulation. J Clim 13: 3721-3727

Esper J, Cook ER, Schweingruber FH (2002) Low-frequency signals in long tree-ring chronologies for reconstructing past temperature variability. Science 295: 2250-2253

Etheridge DM, Steele LP, Langenfelds RL, Francey RJ, Barnola JM, Morgan VI (1996) Natural and anthropogenic changes in atmospheric CO_2 over the last 1000 years from air in Antarctic ice and firn. J Geophys Res 101: 4115-4128

Farquhar GD, von Caemmerer S, Berry JA (1980) A biochemical model of photosynthetic CO_2 assimilation in leaves of C_3 species. Planta 149: 78-90

Foley J (1995) An equilibrium model of the terrestrial carbon budget. Tellus 47B: 310-319

Folland CK, Karl TR, Christy JR, Clarke RA, Gruza GV, Jouzel J, Mann ME, Oerlemans J, Salinger MJ, Wang SW (2001) Observed climate variability and change. In: Houghton JT, Ding Y, Griggs D, Noguer M, van der Linden P, Dai X, Maskell K, Johnson CA (eds) Climate Change 2001: The Scientific Basis. Contribution of Working Group I to the Third Assessment Report of the Intergovernmental Panel on Climate Change, Cambridge University Press, Cambridge, United Kingdom, pp 99-181

Francey RJ, Allison CE, Etheridge DM, Trudinger CM, Enting IG, Leuenberger M, Langenfelds RL, Michel E, Steele LP (1999) A 1000 year high precision record of $\delta^{13}C$ in atmospheric CO_2. Tellus Ser B 51: 170-193

Friedli H, Loetscher H, Oeschger H, Siegenthaler U, Stauffer B (1986) Ice core record of the $^{13}C/^{12}C$ ratio of atmospheric carbon dioxide in the past two centuries. Nature 324: 237-238

Friedlingstein P, Bopp L, Ciais P, Fairhead JLDL, LeTreut H, Monfray P, Orr J (2000) Positive feedback of the carbon cycle on future climate change. Tech Rep 19, Note du Pole de Modelisation, Institute Pierre Simon Laplace, France

Haigh JD (1996) The impact of solar variability on climate. Science 272: 981-984

Hansen J, Lacis A, Rind D, Russell G, Stone P, Fung I, Ruedy R, Lerner J (1984) Climate sensitivity: analysis of feedback mechanisms. Climate Processes and Climate Sensitivity, vol Geophysical Monograph 29, American Geophysical Union, pp 130-163

Haxeltine A, Prentice IC (1996) BIOME 3: an equilibrium terrestrial biosphere model based on ecophysiological constraints, resource availability and competition among plant functional types. Global Biogeochem Cycles 10: 693-703

Hendy EJ, Gagan MK, Alibert CA, McCulloch MT, Lough JM, Isdale PJ (2002) Abrupt decrease in tropical Pacific sea surface salinity at end of Little Ice Age. Science 295: 1511-1514

Hooss G, Voss R, Hasselmann K, Maier-Reimer E, Joos F (2001) A nonlinear impulse response model of the coupled carbon cycle-climate system (niccs). Clim Dyn 18: 189-202

Houghton RA (1999) The annual net flux of carbon to the atmosphere from changes in land use 1850-1990. Tellus Ser B 51: 298-313

Hu FS, Ito E, Brown TA, Curry BB, Engstrom DR (2001) Pronounced climatic variations in Alaska during the last two millennia. Proc Natl Acad Sci USA 98: 10,552-10,556

Huang S, Pollack HN, Shen P (2000) Temperature trends over the past five centuries reconstructed from borehole temperatures. Nature 403: 756-758

Hulme M, Osborn T, Johns T (1998) Precipitation sensitivity to global warming: comparison of observations with HadCM2 simulations. Geophys Res Lett 25: 3379-3382

Indermühle A, Stocker TF, Joos F, Fischer H, Smith H, Wahlen M, Deck B, Mastroianni D, Tschumi J, Blunier T, Meyer R, Stauffer B (1999) Holocene carbon-cycle dynamics based on CO_2 trapped in ice at Taylor Dome, Antarctica. Nature 398: 121-126

Johnsen SJ, Dahl-Jensen D, Gundestrup N, Steffensen JP, Clausen HB, Miller H, Masson-Delmotte V, Sveinbjörnsdottir AE, White J (2001) Oxygen isotope and palaeotemperature records from six Greenland ice stations: Camp Century, Dye-3, GRIP, GISP2, Renland and NorthGRIP. J Quat Sci 16: 299-307

Jones PD (1994) Hemispheric surface air temperature variations: a reanalysis and an update to 1993. J Clim 7: 1794-1802

Jones PD, Briffa KR, Barnett TP, Tett SFB (1998) High-resolution palaeoclimatic records for the last millennium: interpretation integration and comparison with general circulation model control-run temperatures. The Holocene 8: 455-471

Jones PD, New M, Parker DE, Martin S, Rigor IG (1999) Surface air temperature and its changes over the past 150 years. Rev Geophys 37: 173-199

Joos F, Bruno M (1996) Pulse response functions are cost-efficient tools to model the link between carbon emissions, atmospheric CO_2 and global warming. Phys Chem Earth 21: 471-476

Joos F, Bruno M, Fink R, Stocker TF, Siegenthaler U, Le Quéré C, Sarmiento JL (1996) An efficient and accurate representation of complex oceanic and biospheric models of anthropogenic carbon uptake. Tellus Ser B 48: 397-417

Joos F, Meyer R, Bruno M, Leuenberger M (1999a) The variability in the carbon sinks as reconstructed for the last 1000 years. Geophys Res Lett 26: 1437-1441

Joos F, Plattner GK, Stocker TF, Marchal O, Schmittner A (1999b) Global warming and marine carbon cycle feedbacks on future atmospheric CO_2. Science 284: 464-467

Joos F, Prentice IC, Sitch S, Meyer R, Hooss G, Plattner GK, Gerber S, Hasselmann K (2001) Global warming feedbacks on terrestrial carbon uptake under the Intergovernmental Panel on Climate Change (IPCC) emission scenarios. Global Biogeochem Cycles 15: 891-907

Kaplan JO (2002) Wetlands at the Last Glacial Maximum: Distribution and methane emissions. Geophys Res Lett 29 2001GL013366

Kawamura K, Nakazawa T, Machida T, Morimot S, Aoki S, Ishizawa M, Fujji Y, Watanabe O (2000) Variations of the carbon isotopic ratio in atmospheric CO_2 over the last 250 years recorded in an ice core from H15, Antarctica. Polar Meteorol Glaciol 14: 47-57

Keigwin LD, Boyle EA (2000) Detecting Holocene changes in thermohaline circulation. Proc Natl Acad Sci USA 97: 1343-1346

Knutti R, Stocker TF, Joos F, Plattner GK (2002) Constraints on radiative forcing and future climate change from observations and climate model ensembles. Nature 416: 719-723

Kreutz KJ, Mayewski PA, Meeker LD, Twickler MS, Whitlow SI, Pittalwala II (1997) Bipolar changes in atmospheric circulation during the Little Ice Age. Science 277: 1294-1296

Lacis A, Hansen J, Sato M (1992) Climate forcing by stratospheric aerosols. J Geophys Res 19: 1607-1610

Lean J, Beer J, Bradley R (1995) Reconstruction of solar irradiance since 1610: implication for climate change. Geophys Res Lett 22: 3195-3198

Leemans R, Cramer W (1991) The IIASA climate database for land areas on a grid with 0.5° resolution. Res Rep RR -91-18. Tech rep International Institute for Applied System Analysis

Leemans R, Eickhout B, Strengers B, Bouwman L, Schaeffer M (2002) The consequences for the terrestrial carbon cycle of uncertainties in land use, climate and vegetation responses in the IPCC SRES scenarios. Science in China (in press)

Leuenberger M (1992) Isotopen-sowie Konzentrationsbestimmungen an CO_2, N_2O, O_2 und N_2 in Luftproben aus polarem Eis. PhD Thesis, University of Bern, Bern, Switzerland

Lloyd J, Farquhar GD (1994) ^{13}C discrimination during CO_2 assimilation by the terrestrialae biosphere. Oecologia 99: 201-215

Lloyd J, Taylor JA (1994) On the temperature dependence of soil respiration. Functi Ecol 8: 315-323

Luterbacher J, Schmutz C, Gyalistras D, Xoplaki E, Wanner H (1999) Reconstruction of monthly NAO and EU indices back to AD 1675. Geophys Res Lett 26: 2745-2748

Mann ME, Bradley RS, Hughes MK (1998) Global-scale temperature patterns and climate forcing over the past six centuries. Nature 392: 779-787

Mann ME, Bradley RS, Hughes MK (1999) Northern Hemisphere temperatures during the past millennium: inferences, uncertainties, and limitations. Geophys Res Lett 26: 759-762

Marchal O, Stocker TF, Joos F (1999a) On large-scale physical and biogeochemical responses to abrupt changes in the Atlantic thermohaline circulation. In: Webb RS, Clark PU (eds) Mechanisms of millennial-scale global climate change vol 112 Geophysical Monograph, American Geophysical Union, Washington, DC

Marchal O, Stocker TF, Joos F, Indermühle A, Blunier T, Tschumi J (1999b) Modelling the concentration of atmospheric CO_2 during the Younger Dryas climate event. Clim Dyn 15: 341-354

Marshall S, Oglesby RJ, Larson JW, Saltzman B (1994) A comparison of GCM sensitivity to changes in CO_2 and solar luminosity. Geophys Res Lett 21: 2487-2490

McGuire AD, Sitch S, Clein JS, Dargaville R, Esser G, Foley J, Heimann M, Joos F, Kaplan J, Kicklighter DW, Meier RA, Melillo JM, Moore III B, Prentice IC, Ramankutty N, Reichenau T, Schloss A, Tian H, Williams LJ, Wittenberg U (2001) Carbon balance of the terrestrial biosphere in the twentieth century: analyses of CO_2, climate and land-use effects with four process-based ecosystem models. Global Biogeochem Cycles 15: 183-206

Meyer R, Joos F, Esser G, Heimann M, Hooss G, Kohlmaier G, Sauf W, Voss R, Wittenberg U (1999) The substitution of high-resolution terrestrial biosphere models and carbon sequestration in response to changing CO_2 and climate. Global Biogeochem Cycles 13: 785-802

Mitchell JFB, Karoly DJ, Hegerl GC, Zwiers FW, Allen MR, Marengo J (2001) Detection of climate change and attribution of causes. In: Houghton JT, Ding Y, Griggs D, Noguer M, van der Linden P, Dai X, Maskell K, Johnson CA (eds) Climate change 2001: the scientific basis. Contribution of Working Group I to the Third Assessment Report of the Intergovernmental Panel on Climate Change, Cambridge University Press, Cambridge, United Kingdom, pp 695-738

Monteith JL (1995) Accomodation between transpiring vegetation and the convective boundary layer. J Hydrol 166: 251-263

Myhre G, Highwood EJ, Shine KP, Stordal F (1998) New estimates of radiative forcing due to well mixed greenhouse gases. Geophys Res Lett 25: 2715-1718

Neftel A, Moor E, Oeschger H, Stauffer B (1985) Evidence from polar ice cores for the increase in atmospheric CO_2 in the past two centuries. Nature 315: 45-47

Pfister C (1999) Wetternachhersage. 500 Jahre Klimavariationen und Naturkatastrophen, 1496-1995. Paul Haupt, Bern, Switzerland

Pfister C, Schwarz-Zanetti G, Wegmann M (1996) Winter-severity in Europe: the fourteenth century. Clim Change 34: 91-108

Plattner GK, Joos F, Stocker TF, Marchal O (2001) Feedback mechanisms and sensitivities of ocean carbon uptake under global warming. Tellus Ser B 53: 564-592

Plattner GK, Joos F, Stocker TF (2002) Revision of the global carbon budget due to changing air-sea oxygen fluxes. Global Biogeochem Cycles (in press)

Prentice IC, Heimann M, Sitch S (2000) The carbon balance of the terrestrial biosphere: Ecosystem models and atmospheric observations. Ecol Appl 10: 1553-1573

Prentice IC, Farquhar GD, Fasham MJ, Goulden MI, Heimann M, Jaramillo VJ, Kheshgi HS, LeQuéré C, Scholes RJ, Wallace DWR (2001) The carbon cycle and atmospheric CO_2. In: Houghton JT, Ding Y, Griggs D, Noguer M, van der Linden P, Dai X, Maskell K, Johnson CA (eds) Climate change 2001: the scientific basis. Contribution of Working Group I to the Third Assessment Report of the Intergovernmental Panel on Climate Change, Cambridge University Press, Cambridge, United Kingdom, pp 183-237

Ramaswamy V, Boucher O, Haigh J, Hauglustaine D, Haywood J, Myhre G, Nakajima T, Shi GY, Solomon S (2001) Radiative forcing of climate change. In: Houghton JT, Ding Y, Griggs D, Noguer M, van der Linden P, Dai X, Maskell K, Johnson CA (eds) Climate change 2001: the scientific basis. Contribution of Working Group I to the Third Assessment Report of the Intergovernmental Panel on Climate Change. Cambridge University Press, Cambridge, United Kingdom, pp 349-416

Reid GC (1997) Solar forcing and global climate change since the mid-17th century. Clim Change 37: 391-405

Robock A, Mao J (1993) The volcanic signal in surface temperature observations. J Clim 8: 1086-1103

Sato M, Hansen JE (1992) Stratospheric aerosol optical depths, 1850-1990. J Geophys Res 98: 22,987-22,994

Schwander J (1996) Gas diffusion in firn. In: Wolff EW, Bales RC (eds) Chemical exchange between the atmosphere and polar snow vol I 43 of NATO ASI, Springer, Heidelberg Berlin New york

Shindell DT, Schmidt GA, Mann ME, Rind D, Waple A (2001) Solar forcing of regional climate change during the Maunder Minimum. Science 294: 2149-2152

Siegenthaler U (2002) CO_2-Konzentrationsmessungen an polaren Eisbohrkernen und Tests mit einer neuen Extraktionsmethode. Diploma Thesis, University of Bern, Switzerland

Siegenthaler U, Oeschger H (1984) Transient temperature changes due to increasing CO_2 using simple models. Ann Glaciol 5: 153-159

Siegenthaler U, Joos F (1992) Use of a simple model for studying oceanic tracer distributions and the global carbon cycle. Tellus Ser B 44: 186-207

Siegenthaler U, Friedli H, Loetscher H, Moor E, Neftel A, Oeschger H, Stauffer B (1988) Stable-isotope ratios and concentration of CO_2 in air from polar ice cores. Ann Glaciol 10: 1-6

Simkin T, Siebert L (1994) Volcanoes of the world, 2 edn, Geoscience Press, Tucson, AZ, USA

Sitch S (2000) The role of vegetation dynamics in the control of atmospheric CO_2 content. PhD Thesis, Lund University, Sweden

Stauffer B, Blunier T, Dällenbach A, Indermühle A, Schwander J, Stocker TF, Tschumi J, Chappellaz J, Raynaud D, Hammer CU, Clausen HB (1998) Atmospheric CO_2 and millennial-scale climate change during the last glacial period. Nature 392: 59-62

Stauffer B, Flückiger J, Monnin E, Schwander J, Barnola JM, Chappellaz J (2002) Atmospheric CO_2, CH_4 and N_2O records over the past 60,000 years based on the comparison of different polar ice cores. Ann Glaciol (in press)

Stocker TF (1998) The sea saw effect. Science 282: 61-62

Svensmark H, Friis-Christensen E (1997) Variation of cosmic ray flux and global cloud coverage - a missing link in solar-climate relationship. J Atmos Solar Terrest Phys 59: 1225-1232

Thompson DWJ, Solomon S (2002) Interpretation of recent Southern Hemisphere climate change. Science 296: 895-899

Thonicke K, Venevsky S, Sitch S, Cramer W (2001) The role of fire disturbance for global vegetation dynamics: coupling fire into a dynamic global vegetation model. Global Ecol Biogeogr 10: 661-677

Trudinger CM, Enting IG, Francey RJ, Etheridge DM, Rayner PJ (1999) Long-term variability in the global carbon cycle inferred from a high precision CO_2 and $\delta^{13}C$ ice core record. Tellus Ser B 51: 233-248

Tschumi J, Stauffer B (2000) Reconstructing past atmospheric CO_2 concentration based on ice-core analyses: open questions due to in situ production of CO_2 in the ice. J Glaciol 46: 45-53

United Nations (1999) The world at six billion. United Nation Population Division, Working paper 154

Voss R, Mikolajewicz U (2001) Long-term climate changes due to increased CO_2 concentration in the coupled atmosphere-ocean general circulation model ECHAM3/LSG. Clim Dyn 17: 45-60

Wanner H, Pfister C, Brazdil R, Frich P, Fruydendahl K, Jonsson T, Kington J, Lamb HH, Rosenorn S, Wishmann E (1995) Wintertime European circulation patterns during the late Maunder Minimum cooling period. Theor Appl Climatol 51: 167-175

Zobler L (1986) A world soil file for global climate modelling. Technical Memorandum, NASA